STARK EFFECT ON EMISSION SPECTRA OF DIATOMIC MOLECULES

by

DANIEL HOLDSWORTH PHELPS
B.A., Reed College, 1960
M.A., Dartmouth College, 1962

A THESIS SUBMITTED IN PARTIAL FULFILMENT OF
THE REQUIREMENTS FOR THE DEGREE OF
DOCTOR OF PHILOSOPHY

in the Department
of
PHYSICS

We accept this thesis as conforming to the
required standard

THE UNIVERSITY OF BRITISH COLUMBIA

April, 1966

In presenting this thesis in partial fulfilment of the requirements for an advanced degree at the University of British Columbia, I agree that the Library shall make it freely available for reference and study. I further agree that permission for extensive copying of this thesis for scholarly purposes may be granted by the Head of my Department or by his representatives. It is understood that copying or publication of this thesis for financial gain shall not be allowed without my written permission.

Department of Physics

The University of British Columbia
Vancouver 8, Canada

Date May 12, 1966

The University of British Columbia

FACULTY OF GRADUATE STUDIES

PROGRAMME OF THE

FINAL ORAL EXAMINATION

FOR THE DEGREE OF

DOCTOR OF PHILOSOPHY

of

DANIEL H. PHELPS

B.A., Reed College, 1960

M.A., Dartmouth College, 1962

THURSDAY, MAY 12, 1966, AT 2:30 P.M.

IN ROOM 303, HENNINGS

COMMITTEE IN CHARGE

Chairman: D. H. Chitty

A. J. Barnard
A. M. Crooker
F. W. Dalby
R. A. Nodwell
E. A. Ogryzlo
R. D. Russell

External Examiner: A. V. Jones
University of Saskatchewan
at
Saskatoon

Research Supervisor: F. W. Dalby

STARK EFFECT IN EMISSION SPECTRA OF DIATOMIC MOLECULES

ABSTRACT

The infuence of an external electric field on atomic or molecular spectra, known as the Stark effect, typically leads to splittings, shifts, broadenings and changes of intensity in spectral lines. The Stark effect on the electronic emission spectra of the OH and CH molecules was studied for external electric up to 68,000 volts/cm. The Stark spectra were produced in the high electric field region of a low pressure glow discharge. (The electric fields were determined from Stark splittings in hydrogen Balmer lines.) From observations of the Stark effect on the molecular spectra the electric dipole moments were determined for the OH molecule in the $^2\Pi$ electronic state and for the CH molecule in both the $^2\Pi$ and $^2\Delta$ electronic states. From transitions to the following levels the values of the dipole moment were found to be:

OH	$^2\Pi_{1/2}$, J = 1/2, v = 0	$1.73_2 \pm 0.02$ Debye
	$^2\Pi_{3/2}$, J = 3/2, v = 0	$1.63_7 \pm 0.03$
	$^2\Pi_{1/2}$, J = 1/2, v = 1	$1.69_2 \pm 0.04$
CH	$^2\Pi_{1/2}$, J = 1/2, v = 0	1.46 ± 0.06
	$^2\Delta$, J = 7/2, v = 0	$1.13 \pm 15\%$

The first reported observation of resolved first order Stark effects on the electronic spectra of a diatomic molecule resulted from this work. The techniques developed in this investigation are well suited

for the study of short lived and chemically reactive molecules in both their ground and excited electronic states.

GRADUATE STUDIES

Field of Study: Molecular Spectroscopy

Elementary Quantum Mechanics	W. Opechowski
Waves	J. C. Savage
Quantum Theory of Solids	R. Barrie
Spectroscopy	A. M. Crooker
Molecular Spectroscopy	F. W. Dalby
Advanced Spectroscopy	A. J. Barnard

PUBLICATIONS

R.W. Christy and D.H. Phelps, "Production of V_3 in KCL by X Rays", Physical Review 124, 1053 (1961).

D.H. Phelps and F.W. Dalby, "Optical Observations of the Stark Effect on OH", Canadian Journal of Physics 43, 144 (1965).

D.H. Phelps and F.W. Dalby, "Experimental Determination of the Electric Dipole Moment of the Ground Electronic State of CH", Physical Review Letters 16, 3 (1966)

ABSTRACT

The electronic emission spectra of the OH and CH molecules in applied electric fields up to 68,000 v/cm have been observed. These spectra show Stark splittings, broadenings and field-induced, parity-forbidden lines. The electric dipole moment of the molecules has been determined for OH in the $^2\pi$ electronic state and CH in both the $^2\pi$ and $^2\Delta$ electronic states from Stark effects on transitions to the following levels:

OH	$^2\pi_{1/2}$, J = 1/2, v = 0	$1.73_2 \pm 0.02$ Debye
	$^2\pi_{3/2}$, J = 3/2, v = 0	$1.63_7 \pm 0.03$
CH	$^2\pi_{1/2}$, J = 1/2, v = 1	$1.69_2 \pm 0.04$
	$^2\pi_{1/2}$, J = 1/2, v = 0	1.46 ± 0.06
	$^2\Delta$, J = 7/2, v = 0	$1.13 \pm 15\%$

Electric fields were determined from Stark splittings in hydrogen Balmer lines. The Stark spectra were produced in the high field region of a low pressure glow discharge. This technique is well suited for the study of short lived and chemically reactive molecules in both their ground and excited electronic states.

TABLE OF CONTENTS

CHAPTER I: INTRODUCTION 1

Footnotes for Chapter I 5

CHAPTER II: THEORETICAL PRELUDE 7

Energy of a diatomic molecule in an electric field ... 7

Matrix elements of the perturbation 8

The perturbation and parity 9

Vector model treatment of Hund's coupling case (a) ... 10

The secular equation for lambda doublet levels 14

Stark effect spectra 15

Rigorous treatment of matrix elements 19

Coupling intermediate between Hund's case (a) and case (b) 25

Parity mixing and transitions between perturbed lambda doublets 27

Second order Stark effects 31

Footnotes for Chapter II 35

CHAPTER III: EXPERIMENTAL DETAILS 36

Electric discharge tube 36

Production of OH and CH electronic emission spectra .. 40

Observing the Stark effect 42

Determination of the electric field strength 43

Footnotes for Chapter III 45

CHAPTER IV: EXPERIMENTAL OBSERVATIONS 46

Stark effect on the OH, $^2\Sigma^+ \rightarrow {}^2\Pi$ band 46

Stark effect on the CH, $^2\Sigma^- \rightarrow {}^2\Pi$ band 54

Stark splittings in the atomic hydrogen Balmer line H_γ 58

Stark effect on the CH, $^2\Delta \rightarrow {}^2\Pi$ band 58

Experimental conditions for spectrograms 62

Measurements 62

Analysis of Stark effect spectra 69

Determination of electric dipole moments 77

Summary 87

Footnotes for Chapter IV 90

CHAPTER V: CONCLUSION AND SUGGESTION FOR FURTHER STUDY 91

Suggestions for further work 91

LIST OF TABLES

TABLE I: Experimental Conditions for Spectrograms used in Figures 63

TABLE II: Observed Stark Splittings in OH, $^2\Sigma^+ \rightarrow {}^2\Pi$ Band and in hydrogen Balmer H_γ 64

TABLE III: Observed and Calculated Positions of field-induced, parity-forbidden lines in the $^2\Sigma^+ \rightarrow {}^2\Pi$, (0,0), band of OH 66

TABLE IV: Observed Stark Splittings in CH, $^2\Sigma^- \rightarrow {}^2\Pi$ Band and in hydrogen Balmer H_γ 68

TABLE V: Simultaneously Observed Stark Splittings in CH and OH $^2\Sigma \rightarrow {}^2\Pi$ Bands 70

TABLE VI: Experimental Conditions for Plates Used to Determine OH and CH Electric Dipole Moments .. 71

TABLE VII: OH Electric Dipole Moments Derived from Stark Splittings 78

TABLE VIII: Corrected Stark Splittings in OH $^2\Sigma^+ \rightarrow {}^2\Pi$ Band 80

TABLE IX: Corrected Low Dispersion Stark Splittings in CH $^2\Sigma^- \rightarrow {}^2\Pi$ Band 83

TABLE X: Corrected, Simultaneous Observed Stark Splittings in CH and OH $^2\Sigma \rightarrow {}^2\Pi$ Bands 85

TABLE XI: Electric Dipole Moments for the OH and CH Molecules 89

LIST OF FIGURES

Figure 2.1: Vector diagram of a diatomic molecule in an electric field, Hund's case (a) 11

Figure 2.2: Stark effect on OH, $P_{12}(1)$ and $P_1(1)$ lines ... 16

Figure 2.3: Zero field and field-induced, parity-forbidden transitions associated with $Q_1(4)$ and $Q_{21}(4)$ lines of OH 18

Figure 2.4: Zero field and field-induced, parity-forbidden transitions between lambda doublets. 29

Figure 2.5: Stark effect on CH, $Q_{1c}(3)$ and $Q_{1d}(3)$ lines .. 32

Figure 3.1: Modified Lo Surdo discharge tube 37

Figure 4.1: Allowed transitions to lowest rotational levels in OH $^2\Pi_{1/2}$ and $^2\Pi_{3/2}$ states 47

Figure 4.2: Stark effect on OH, $^2\Sigma^+ \rightarrow {}^2\Pi$, (0,0) band 48

Figure 4.3: Stark effect on OH 52

Figure 4.4: Stark effect on OH, $^2\Sigma^+ \rightarrow {}^2\Pi$, (1,1) band 53

Figure 4.5: Stark effect on CH, $^2\Sigma^- \rightarrow {}^2\Pi$, (0,0) band 55

Figure 4.6: Stark effect on CH, $^2\Sigma^- \rightarrow {}^2\Pi$, (0,0) band for three values of electric field 57

Figure 4.7: Stark effect on hydrogen Balmer H_γ 59

Figure 4.8: Stark effect on CH, $^2\Delta \rightarrow {}^2\Pi$ band 60

Figure 4.9: Corrected Stark splitting, $\Delta\nu'$, vs. electric field strength, E, for OH, $R_2(1)$, (0,0) line . 79

Figure 4.10: First-order Stark splitting of CH, $P_{12}(1)$ line vs. first-order Stark splitting of OH, $R_2(1)$ line 86

ACKNOWLEDGEMENTS

I wish to thank Professor F. W. Dalby, my research director, for his helpful assistance and criticism throughout this work.

This work was supported by the National Research Council of Canada.

CHAPTER I

INTRODUCTION

The influence of an external electric field on atomic or molecular spectra, known as the Stark effect, typically produces splittings, shifts, broadenings and changes in intensity in spectral lines. This study will be concerned with the Stark effect on the electronic emission spectra of diatomic molecules. Observations of the Stark effect on such molecular spectra provide a means of determining the electric dipole moment of a molecule.

The Stark effect on an atomic spectrum was first observed for hydrogen. It was observed independently by Stark[1] and by LoSurdo[2] in 1913. The Stark effect on the hydrogen Balmer lines provided a successful test for the Bohr theory of the hydrogen atom.[3] The Stark effect on various atomic spectra was studied extensively until the mid-1930's. (A review article by Verleger provides many references on this subject.[4])

Several theoretical studies of the Stark effect on molecular band spectra were reported during the 1920's.[4] In 1931, W. G. Penny published a theoretical paper covering the Stark effect on both symmetric top and asymmetric top molecules.[5] In his introduction he said that with the increasing importance of the subject of band spectra his study had been undertaken ". . . in the hope that the experimental difficulties involved in testing the results would soon be overcome."[5] Penny specifically stated in his conclusion that for a diatomic molecule

in an electronic state with a component of angular momentum along the internuclear axis (i.e. a Π, Δ, etc. state) and with a non-vanishing electric dipole moment ". . . there will be a splitting, quadratic at first and linear as soon as the energy shifts become large compared with the natural λ-doubling intervals."[5] Penny also specifically stated that there would be no appreciable contribution to the Stark effect from electronic Σ states (for which there is no component of angular momentum along the internuclear axis).

Contemporary to Penny's work, numerous experimental studies were made of the Stark effect on the band spectra of the hydrogen molecule.[6-11] The observed shifts in frequency obeyed a quadratic relationship to the applied electric field. (The observed transitions did involve an electronic Π state but since from symmetry the H_2 molecule can have no permanent electric dipole moment only a second order Stark effect was observed.) The N_2^+ $^2\Sigma - ^2\Sigma$ (0,0) band at 3914Å and (0,1) band at 4278Å were observed in electric fields up to 280 kV; no splittings were observed. (Notice that the N_2^+ molecule can have no permanent electric dipole moment. Thus it is not surprising that no appreciable Stark effect was observed.) Experiments which could have shown a first order Stark effect were made on the CO^+ comet tail band[8] with electric fields up to 280 kV/cm and on the CO bands[12] at 4835, 4511, 4393, and 4123Å with electric fields of 115 kV/cm. Both of these experiments showed neither displacements nor splittings. These negative results could be due to the rather low dispersion used. (The greatest

dispersion reported was 4Å/mm used in the study of the Stark effect on CO.) Also, for the CO molecule it is now known from microwave measurements that the dipole moment is only 0.112 Debye[13] in the ground state.

Herzberg[14] in discussing the first order Stark effect used the example of a $J = 1$, $^1\Pi$ level; an electric dipole moment of 1 Debye; and an electric field of 10 kV/cm which corresponds to an overall splitting of 0.168 cm^{-1}. He said: "No such splittings have yet been observed even though they are within reach of ordinary spectroscopic methods."[14]

The results reported here include the first reported observations of first order Stark splittings in molecular electronic spectra.[15] This work provided the only published experimental value of the electric dipole moment of the CH molecule.[16] Also, at its time of publication the value of the electric dipole moment of the OH molecule determined from this work[17] was more accurate than earlier values determined using microwave techniques.

Knowledge of the electric dipole moment of a molecule is important because of fundamental interest and also as a test for theoretically computed wave functions. Recently, knowledge of the electric dipole moment of molecules has also become important to radio astronomers. For example, to determine the density of OH molecules from observed microwave absorption[18] in the interstellar medium the electric dipole moment must be known. The dipole moment of the CH molecule is also currently of importance in estimating the strength of the lambda doublet transi-

tion for the J = 1/2 level of the $^2\Pi$ electronic ground state. Douglas and Elliott[19] have determined this lambda doubling to be 3,400 Mc/sec.

The Stark effect on the spectra reported here was produced in a modified LoSurdo[2] type discharge tube. This technique is particularly useful for studying the Stark effect on the spectra of short lived and chemically reactive species in both their ground and electronically excited states. Molecular electric dipole moments have been determined from measurements of dielectric constant, from microwave observations of the second order Stark effect on lambda doublet levels and from molecular beam experiments using resonance techniques. However, these conventional techniques are generally applicable only to stable molecules in their electronic ground state.

In addition to the work reported here the LoSurdo technique has also been successfully applied to determine the electric dipole moment of the NH molecule in three electronic excited states:[20] A $^3\Pi$, a $^1\Delta$, and c $^1\Pi$. Presently this technique is being used to study the Stark effect on the spectra of the HCl^+ molecule.[21]

Footnotes for Chapter I

1. J. Stark, Ann. Physik 43, 965 (1914).

2. A. Lo Surdo, Attii. Accad. Lincei 22, 665 (1913).

3. See for example, E. U. Condon and G. H. Shortley, The Theory of Atomic Spectra (Cambridge University Press, Cambridge, England, 1935), p. 397.

4. H. Verleger, Ergib. exakt. Naturwiss. 18, 99 (1939).

5. W. G. Penny, Phil. Mag. 11, 602 (1931).

6. J. K. L. McDonald, Proc. Roy. Soc. (London) 123, 103 (1929).

7. _____, Proc. Roy. Soc. (London) 131, 146 (1931).

8. W. Rave, Z. Physik 94, 72 (1935).

9. H. Snell, Trans. Roy. Soc. (London) 234, 115 (1935).

10. H. Hasunuma, Proc. Phys.-Math. Soc. Japan 18, 469 (1936).

11. J. S. Foster, D.C. Jones, and S. M. Neamtam, Phys. Rev. 51, 1029 (1935).

12. B. Svenson, Z. Physik 107, 485 (1937).

13. C. A. Burrus, J. Chem. Phys. 28, 427 (1958).

14. G. Herzberg, Molecular Spectra and Molecular Structure. I. Spectra of Diatomic Molecules (D. Van Nostrand Co., New York, 1950), Second edition, p. 308.

15. D. H. Phelps and F. W. Dalby, paper presented at the Symposium on Molecular Structure and Spectroscopy, The Ohio State University, Columbus, Ohio, June, 1963.

16. D. H. Phelps and F. W. Dalby, Phys. Rev. Letters 16, 3 (1966).

17. D. H. Phelps and F. W. Dalby, Can. J. Phys. 43, 144 (1965).

18. S. Weinreb, A. H. Barrett, M. L. Meeks, and J. C. Henry, Nature 200, 829 (1963).

19. A. E. Douglas and G.A. Elliott, Can. J. Phys. 43, 496 (1965).

20. T. A. R. Irwin and F. W. Dalby, Can. J. Phys. 43, 1766 (1965).

21. Mr. S. Y. Wong is completing his M. Sc. thesis at U.B.C. on this topic under the direction of Dr. F. W. Dalby.

CHAPTER II

THEORETICAL PRELUDE

One observes that the Stark effect alters both the frequency and intensity of electronic emission spectral lines. As we will see, this is the consequence of a perturbation of the rotational energy levels due to the interaction of the applied electric field and the average value of the electric dipole moment in the direction of the electric field. All the observed features of the Stark effect on the spectra of a diatomic molecule can be predicted and the mathematical relationships needed to determine electric dipole moments will be obtained by answering the following questions: 1) How does one describe the interaction of the applied electric field and the charge distribution of the molecule? 2) Treating this interaction as a perturbation using quantum mechanics, when does this interaction have a nonzero matrix element? 3) How does the perturbation alter the energy of the molecule? 4) How does the perturbation effect the character of the molecular energy levels?

Energy of a diatomic molecule in an electric field

The energy associated with a distribution of electrons interacting with an external electric field can be found by summing the contribution due to each charge. For the diatomic molecule let us take the co-ordinate origin at the center of positive charge. The perturbation energy will be of the form:

$$V = -\sum_i e\vec{r}_i \cdot \vec{E} \ , \qquad (2.1)$$

where e is the electronic charge, $\vec{r}_i$ is the position of the i th electron, and $\vec{E}$ is the electric field strength. Equation (2.1) will now be rewritten in terms of the electric dipole moment. First, since the molecule is axially symmetric, only the component of the position vector along the internuclear axis, ζ_i, will contribute to expression (2.1). Thus, the contribution to the energy from an individual electron may be written: $e\zeta_i\vec{n}\cdot\vec{E}$, where $\vec{n}$ is a unit vector along the internuclear axis. Second, we also see that equation (2.1) could be evaluated by first summing over $e\vec{r}_i$, since the electric field vector may be taken as a constant, and then the dot product could be taken. Therefore, equation (2.1) will be written:

$$V = (-e\sum_i \zeta_i)\vec{n}\cdot\vec{E} = -\vec{\mu}\cdot\vec{E} \ . \qquad (2.2)$$

We see this expression is consistent with a description of the interaction energy which uses a dipole moment, $\vec{\mu}$, of magnitude $(e\sum_i \zeta_i)$ directed along the internuclear axis.

Matrix elements of the perturbation energy

The total wave function describing an energy level can be taken as the product of three factors, one an electronic eigenfunction, one relating to vibration and one to rotation. For the experimental problem studied here the matrix elements of the perturbation will be important only when the separation of two otherwise appropriate energy levels is comparable to the perturbation energy. Thus we conclude the matrix elements of the perturbation between two levels will only be important if the two levels belong to the same electronic and vibrational level.

They then have the form:

$$V_{12} = \langle \psi_e^* \psi_v^* \psi_{r_1}^* | \ (-e\Sigma_i \zeta_i)\vec{n}\cdot\vec{E} | \ \psi_e \psi_v \psi_{r_2} \rangle \ . \qquad (2.3)$$

Taking the direction of the electric field as the z-axis of a co-ordinate system fixed in space we can replace the dot product, $\vec{n}\cdot\vec{E}$, by $n_z E$, where n_z is the projection of the unit vector $\vec{n}$ along the direction of $\vec{E}$, the electric field, and E is the magnitude of the electric field. Noting that the electronic and vibrational wave functions are the same in the initial and final state equation (2.3) becomes:

$$V_{12} = \langle \alpha v | \ (-e\Sigma_i \zeta_i) | \alpha v \rangle \langle \psi_{r_1}^* | \ n_z E \ | \psi_{r_2} \rangle \ , \qquad (2.4)$$

where the α and the v characterize the electronic and vibrational state. The first factor in expression (2.4) is the quantum mechanical expression for the electric dipole moment in the particular electronic and vibrational state. We will be studying diatomic molecules for which there is a net dipole moment. For this situation equation (2.4) indicates that the behavior of the second factor, which involves the quantum mechanical average of the z-component of a vector, will determine whether a Stark effect will be observed.

The perturbation and parity

The initial and final rotational levels indicated above must have opposite parity for the matrix element of the perturbation energy to be nonzero. For this argument we can write the matrix element as:

$$V_{12} = -\mu E \langle \psi_1^* | \ \cos\theta \ | \psi_2 \rangle \ , \qquad (2.5)$$

where θ is the angle between the electric field and the dipole moment lying along the internuclear axis. If we now perform a reflection through the origin, x becomes -x, y becomes -y, z becomes -z, and cos θ becomes -cos θ. That is, cos θ has negative parity. For the value of V_{12} to be nonzero it must not change for such a reflection. Thus we conclude that ψ_1 and ψ_2 must have opposite parity. The perturbation discussed here will have the greatest effect on rotational levels which are degenerate with respect to parity. Lambda doublet rotational levels occurring for electronic Π, Δ, etc. states closely approximate such a situation.

Vector model treatment of Hund's coupling case (a)

Figure 2.1 shows the vector model for Hund's coupling case (a) for which the electronic motion is strongly coupled to the internuclear axis. Using this vector model the matrix elements shown in equation (2.4) can be found classically for a lambda doublet level. This discussion is presented here since it allows us to easily anticipate the essential features of the Stark effect on the spectra of a diatomic molecule. (The results found here will be derived rigorously later.)

In Figure 2.1, $\vec{J}$, the total angular momentum is the vector sum of $\vec{N}$, the rotational angular momentum of the nuclei and of $\vec{\Omega}$, the angular momentum of the electrons taken along the internuclear axis. $\vec{\Omega}$ is composed of $\vec{\Sigma}$, the projection of the electronic spin angular momentum and of $\vec{\Lambda}$, the projection of the electronic orbital angular momentum, each taken along the inter-

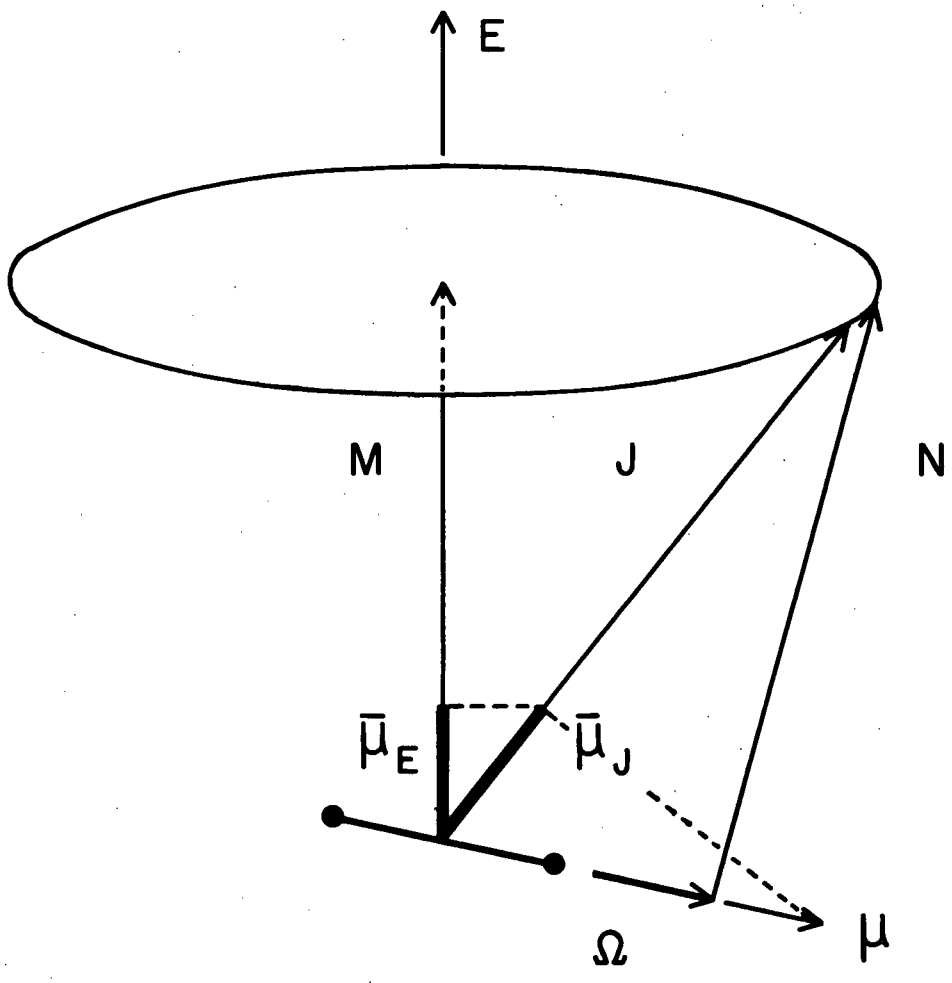

Figure 2.1. Vector diagram of a diatomic molecule in an electric field, Hund's case (a).

nuclear axis. (This Σ should not be confused with the symbol for an electronic state in which the orbital angular momentum is zero which corresponds to an atomic S state.) The vector diagram also shows $\vec{\mu}$, the electric dipole moment, $\vec{E}$, the electric field strength, and $\vec{M}$, the component of $\vec{J}$ in the direction of $\vec{E}$.

Using this vector model the perturbation energy will be found as follows. (This treatment is similar to Herzberg's[1] discussion of the Zeeman effect in Hund's case (a).) The perturbation energy is the product of the magnitude of the electric field strength, E, and of $\overline{\mu_E}$, the average value of the electric dipole moment in the direction of the electric field. This average value of the dipole moment is found by first finding the average value of $\vec{\mu}$ along $\vec{J}$ since Ω (and $\vec{\mu}$) precess rapidly about the direction of $\vec{J}$. This average value along $\vec{J}$, $\overline{\mu_J}$, is then averaged along the direction of $\vec{E}$. Thus we write:

$$\overline{\mu_J} = \mu \cos(\vec{\mu}, \vec{J}) = \mu \frac{\Omega}{|\vec{J}|} \tag{2.6}$$

$$\overline{\mu_E} = \overline{\mu_J} \cos(\vec{J}, \vec{E}) = \overline{\mu_J} \frac{M}{|\vec{J}|} \tag{2.7}$$

If we now use equation (2.6) to replace the factor $\overline{\mu_E}$ in equation (2.7) we find:

$$\overline{\mu_E} = \mu \frac{M\Omega}{|\vec{J}|^2} = \mu \frac{M\Omega}{J(J+1)} , \tag{2.8}$$

since the magnitude of the vector J can be replaced by $(J(J+1))^{\frac{1}{2}}$, (in units of $h/2\pi$) J being the quantum number for the total angular momentum. Using equation (2.8) we can now write the perturbation energy as:

$$V_{12} = -\overline{\mu_E} E = -\mu E \frac{M\Omega}{J(J+1)} . \tag{2.9}$$

Thus the perturbation energy can be found in terms of the magnitudes of the electric dipole moment and of the electric field strength; and the quantum numbers for the total angular momentum and its projections along the direction of the electric field and along the internuclear axis.

From equation (2.9) we can conclude the following: The number of Stark components will increase with increasing angular momentum. (This is due to the factor M which will assume values J, J-1, . . ., -J.) The separation between adjacent Stark components of an energy level will decrease due to the factor of J(J+1) in the denominator of equation (2.9). Thus the Stark splittings will be resolved only for lower values of J. We can also conclude that an electronic state having no component of electronic angular momentum along the internuclear axis will contribute nothing to the first order Stark effect since this situation corresponds to $\Lambda = 0$. For example, in an electronic $^2\Sigma$ state the orbital angular momentum is zero and the spin angular momentum is coupled to the axis of nuclear rotation resulting in $\Lambda = 0$. One could also conclude that a $^2\Sigma$ state would not contribute to a first order Stark effect since each of the rotational levels has definite parity.

More precisely the spin doublet levels in a $^2\Sigma$ electronic state have the same parity and thus cannot perturb each other. There will be perturbations between spin doubled rotational levels of opposite parity. However for the hydride molecules studied here the adjacent rotational levels of opposite parity are so widely separated in energy that they contribute only a

very small second order term. This is also true for the perturbation between neighboring rotational levels in the $^2\pi$ and $^2\Delta$ states investigated here. Further discussion of the interaction between adjacent rotational levels will be reserved for a specific section below.

The secular equation for lambda doublet levels

The energy eigen-values for a lambda doublet will now be given using the matrix elements found above for a perturbation due to the interaction of a permanent molecular electric dipole with an applied electric field. Using these energy eigen-values we will be able to predict: 1) resolved first order Stark splittings for lower values of J, 2) Stark broadenings, and 3) electric field-induced, parity-forbidden lines.

The eigen-values for the energy of perturbed lambda doublet levels are given by the roots of ϵ^1 the following equation:

$$\det \begin{vmatrix} V_{11} - \epsilon^1 & V_{12} \\ V_{21} & V_{22} - \epsilon^1 \end{vmatrix} = 0 . \qquad (2.10)$$

The off diagonal elements, $V_{12} = V_{21}$, are given in equation (2.9). V_{11} and V_{22} are the energies of the two unperturbed lambda doublets. If we take the zero of energy as midway between the two unperturbed levels and write their separation $V_{11} - V_{22} = \lambda$, the solution to equation (2.10) may be written as:

$$\epsilon^1 = \pm \sqrt{(\lambda/2)^2 + (V_{12})^2} . \qquad (2.11)$$

From this solution we see that both levels of the lambda doublet

will split into as many components as there are values of |M|. We may relate this energy degeneracy for values of M and -M to the appearance of a factor of M^2 under the square root due to the matrix element of the perturbation being squared. This M degeneracy is a consequence of Kramers' theorem which states that for a system with a half integral value of the sum of the spin of the particles "...in an arbitrary electric field, all levels must be doubly degenerate . . . ."[2] Since all the molecules studied here were in states having total electronic spin of 1/2, the Kramers' degeneracy in M would remain even for an arbitrary electric field.

Stark effect spectra

The perturbation between associated lambda doublet levels of opposite parity will cause the perturbed energy levels to be mixed. The extent of the mixing will be discussed in detail below, but for the present knowing that the perturbed levels have mixed parity we can predict the essential feature of the Stark effect on the spectra of a diatomic molecule.

A strict selection rule for electric dipole transitions is that states of positive parity combine only with states of negative parity and vice versa. The parity mixing due to the perturbation resulting from the electric field will lead to transitions which are forbidden in the absence of the electric field. Figure 2.2 shows two examples of parity forbidden transitions which are induced by the electric field. The transitions shown in the figure are for the OH molecule and corresponding lines

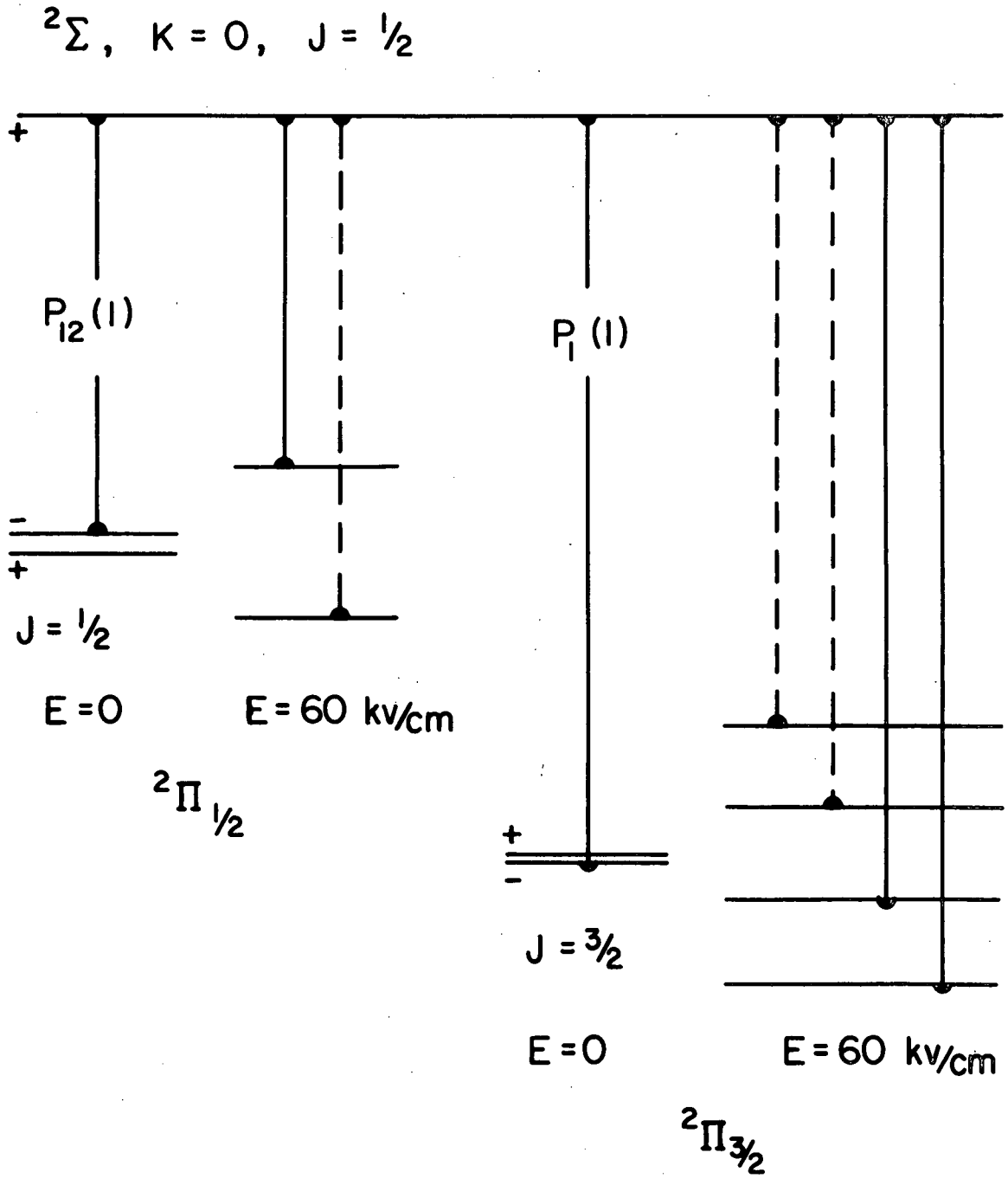

Figure 2.2. Stark effect on OH, $P_{12}(1)$ and $P_1(1)$ lines. Broken lines indicate forbidden transitions. Lambda doubling and Stark splittings are drawn to the same scale for both rotational levels.

show resolved first order Stark splittings. The splittings are first order in the applied electric field because the perturbation energy is several times larger than the separation of the lambda doublet levels. Transitions to rotational levels with larger values of J did not show resolved Stark splittings for the following reasons: As J increases the lambda doubling and the number of Stark components also increase. Since the separation of the Stark components decreases with increasing J, the Stark effect will generally broaden all transitions except those to the lowest rotational levels. When the lambda doubling becomes somewhat larger than the perturbation, the lambda doublet components will still be of mixed parity. Thus for higher rotational lines the forbidden line will appear quite narrow and well separated from the allowed line. Figure 2.3 shows an example of the zero field and field induced transitions for the $Q_1(4)$ and $Q_{21}(4)$ lines of the $^2\Sigma^+ \rightarrow {}^2\Pi$, (0,0) band of the OH molecule. The field-induced, parity-forbidden line associated with the $Q_{21}(4)$ line was obscured by the allowed component of the $Q_1(4)$ line.

In conclusion we see that the Stark effect will result in resolved splittings, broadenings, and clearly separated field-induced, parity-forbidden lines for electronic transitions if either the initial or final level is degenerate in energy with respect to parity. Before discussing the Stark effect on spectra resulting from transitions between electronic states for which both rotational levels are degenerate, e.g. $^2\Delta \rightarrow {}^2\Pi$, the matrix elements for the perturbation involving the electric

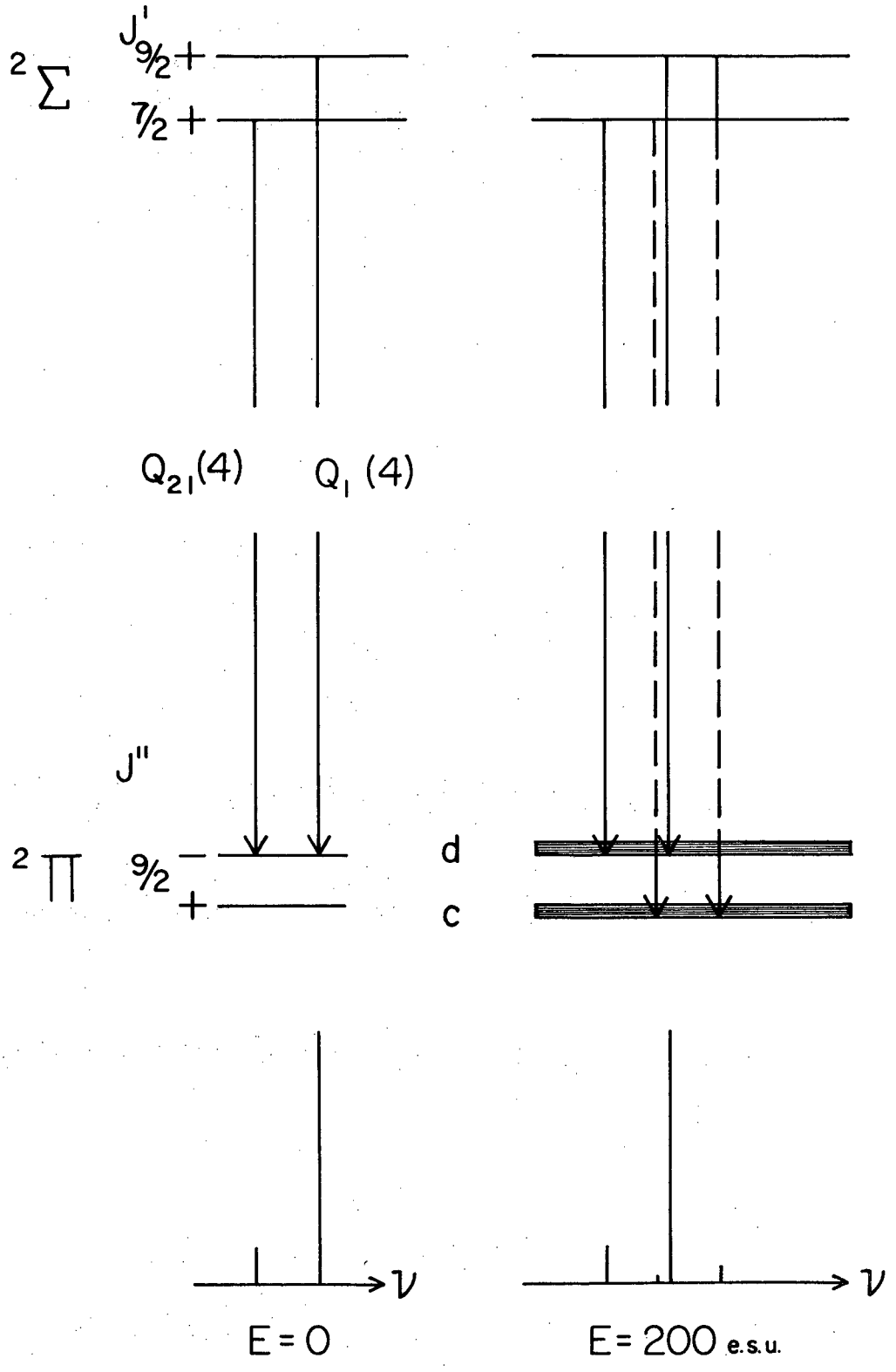

Figure 2.3. Zero field and field-induced, parity-forbidden transitions associated with $Q_1(4)$ and $Q_{21}(4)$ lines of OH, $^2\Sigma^+ \rightarrow {}^2\pi$, band. Broken lines indicate field induced transitions.

field and the electric dipole moment will be found rigorously. These rigorouslyalues will confirm the correctness of the vector model result for the matrix elements. From the following section we will also see what corrections are to be made when a rotational level does not belong to pure Hund's case (a) coupling.

Rigorous treatment of matrix elements

In the initial discussion of the matrix elements for the perturbation energy of a molecule with a permanent electric dipole moment in an applied electric field were given by:

$$V_{12} = \langle \alpha\, v \mid (-e \sum_i \zeta_i) \mid \alpha\, v \rangle \langle \psi^*_{r_1} \mid n_z E \mid \psi_{r_2} \rangle. \qquad (2.4)$$

We recall that the first factor represents the electric dipole moment for a particular electronic and vibrational state characterized by α and v. The electric field has magnitude E, and is parallel to the z-axis of a co-ordinate system fixed in space. The unit vector $\vec{n}$ is parallel to the internuclear axis and n_z is the component along the z-axis (field direction). Thus, as stated in the introduction to this chapter, the perturbation causing the Stark effect does correspond to the interaction of the electric field and the average value of the electric dipole moment in the direction of the electric field. The dependence of the matirx elements of the perturbation on this averaging can be emphasized by writing:

$$V_{12} \quad -\mu E \langle \psi^*_1 \mid n_z \mid \psi_2 \rangle. \qquad (2.12)$$

We have already shown that the initial and final rotational eigen-functions must have opposite parity. We will now find the remaining conditions on these eigen-functions for nonzero matrix

elements. Essentially we wish to determine when the quantum mechanical average of the z-component of a vector is nonzero. The nonzero values of $\langle n_z \rangle$ for Hund's coupling case (a) will now be discussed.

In Hund's coupling case (a) the electronic motion is strongly coupled to the internuclear axis. The good quantum numbers for this coupling case are: α, Λ, J, M. α denotes the assembly of quantum numbers associated with the electronic term with the exception of Λ. Λ corresponds to the component of the electronic orbital angular momentum along the internuclear axis. J is the total angular momentum quantum number and M denotes the component of the total angular momentum in the direction of the external field. α has been absorbed in the expression for the electric dipole moment displayed in equation (2.4). Matrix elements between electronic states with different values of Λ (which are widely separated in energy compared to the perturbation) will not contribute to the Stark effect. For this reason the perturbation will be discussed for initial and final states belonging to the same electronic and vibrational state and α and Λ will not be indicated explicitly in the following discussion.

The matrix elements in equation (2.12) are identical with the matrix elements for electric dipole radiation polarized along the z-axis. Hence the additional restrictions on the matrix elements given in equation (2.12) are seen from a discussion of the appropriate selection rules for electric dipole transitions and for Hund's case (a) coupling. The following general rules for electric dipole transitions are relevant:[3]

For the total angular momentum quantum number, J,
$$\Delta J = \pm 1, 0$$
except that $J = 0$ does not combine with $J = 0$.

States of odd parity combine only with states of even parity and vice versa.

The other general selection rules for identical nuclei and for nuclei of equal charge do not apply as such molecules would not have a permanent electric dipole moment and therefore would show no first order Stark effect. The following selection rules apply to both Hund's coupling case (a) and case (b). For Hund's coupling case (b) the electronic spin is weakly coupled to the internuclear axis. (Hund's case (b) will be discussed in detail below.)

For Λ, the component of the electronic orbital angular momentum: $\Delta\Lambda = \pm 1,0$

For the total electronic spin quantum number, S,
$$\Delta S = 0$$

The remaining selection rules needed to complete the discussion of the perturbation matrix elements in Hund's case (a) apply when both states belong to case (a):[3]

The component of the electronic spin along the internuclear axis does not alter, i.e.:
$$\Delta\Sigma = 0$$

For the component of the total angular momentum along the internuclear axis:
$$\Delta\Omega = \pm 1, 0$$

As we have restricted our interest to initial and final states having the same value of Λ, only states with the same value of Ω may combine since $\Omega = \Lambda + \Sigma$ and $\Delta\Sigma = 0$. Specifically for matrix elements of n_z, $\Delta M = 0$. Using these facts we find that the necessary nonzero matrix elements for the average of a vec-

tor in the direction of the electric field in Hund's case (a) are:[4]

$$\langle \Lambda J\ M|\ n_z|\ \Lambda\ J\ M\rangle = \langle \Lambda\ J|\ n_z|\ \Lambda\ J\rangle\ M$$
$$\langle \Lambda J\ M|\ n_z|\ \Lambda\ J-1\ M\rangle = \langle \Lambda\ J|\ n_z|\ \Lambda\ J-1\rangle \sqrt{(J^2 - M^2)}$$
$$\langle \Lambda J-1\ M|\ n_z|\ \Lambda\ J\ M\rangle = \langle \Lambda\ J-1|\ n_z|\ \Lambda\ J\rangle \sqrt{(J^2 - M^2)} \qquad (2.13)$$

Although the parity of the states is not shown here explicitly, the initial and final state must have opposite parity. The first relationship will be used for lambda doublets and the other two will be used in finding second order effects due to neighboring rotational levels. The factors in equation (2.13) which depend only on J and Λ are given by:[4]

$$\langle \Lambda J\ |\ n_z|\ \Lambda\ J\rangle = \frac{\Lambda}{J(J+1)}$$
$$\langle \Lambda J|\ n_z|\ \Lambda\ J-1\rangle =$$
$$= \langle \Lambda\ J-1|\ n_z|\ \Lambda\ J\rangle = \frac{1}{J}\sqrt{\frac{(J - \Lambda)(J + \Lambda)}{(2J - 1)(2J + 1)}} \qquad (2.14)$$

We can see for example that the vector model result for the perturbation matrix elements between lambda doublets given in equation (2.9) is correct. The corresponding quantum mechanical result is obtained from equation (2.12) using the first relationship in equation (2.13) and (2.14) and one obtains:

$$V_{12} = -\mu E \frac{M\Lambda}{J(J+1)}\ , \qquad (2.15)$$

in agreement with the vector model result.

In Hund's coupling case (b) the electronic spin angular momentum is weakly coupled to the internuclear axis. To find the matrix elements of the perturbation for Hund's case (b) we need to know which quantum numbers are good and which selection

rules apply specifically. The good quantum numbers are α, Λ, K, S, J, M, and parity. As above; α denotes the assembly of quantum numbers describing the electronic term with the exception of Λ which corresponds to the projection of the electronic angular momentum on the internuclear axis; J is the total angular momentum quantum number; and M corresponds to the projection of the total angular momentum along the direction of the applied electric field. The quantum number K denotes the total angular momentum apart from spin. K is composed of electron orbital angular momentum along the internuclear axis and angular momentum due to rotation of the nuclei. The total electron spin angular momentum is denoted by S.

The selection rules given above for the general situation of electric dipole transitions and for both Hund's case (a) and case (b) can be immediately applied. Since we are only interested in the interaction of neighboring rotational levels which both correspond to case (b) coupling we only need the appropriate selection rule for K, i.e.:[3]

$$\Delta K = \pm 1, 0$$

except for $\Sigma - \Sigma$ transitions for which $\Delta K = 0$ is forbidden.

In complete detail the desired matrix element of n_z for case (b) coupling would be written: $\langle \alpha \Lambda K S J M | n_z | \alpha' \Lambda' K' S' J' M' \rangle$. One may summarize the discussion above and greatly simplify the matrix element by saying: $\alpha = \alpha'$, $\Lambda = \Lambda'$, $S = S'$ and the parity although not shown explicitly must be opposite in the initial and final states. Let us drop the quantum numbers which are not needed explicitly and use the selection rule for n_z, i.e. $\Delta M = 0$. The

desired matrix element thus simplifies to:

$$\langle \Lambda\ K\ S\ J\ M|\ n_z\ \ \Lambda\ K'\ S\ J'\ M\rangle .$$

These matrix elements will be found by first neglecting spin and then using the appropriate formulas for finding the matrix elements relating to the addition of angular momenta. Considering only Λ and K the nonzero matrix elements are:[5]

$$\langle \Lambda\ K|\ n_z|\ \Lambda\ K\rangle = \frac{\Lambda}{K(K+1)}$$

$$\langle \Lambda\ K|\ n_z|\ \Lambda\ K-1\rangle = \langle \Lambda\ K-1|\ n_z\ |\Lambda\ K\rangle =$$

$$= \frac{1}{K}\sqrt{\frac{(K-\Lambda)(K+\Lambda)}{(2K-1)(2K+1)}} . \qquad (2.16)$$

We will be interested specifically in $^2\Sigma$ electronic states which always obey case (b) coupling. As noted above for such a $\Sigma-\Sigma$ transition $\Delta K = 0$ is forbidden and thus the first expression in (2.16) is automatically zero. This agrees with the vector model result given above. For an electronic Σ state, $\Lambda = 0$ and the remaining expression in (2.16) reduces to:

$$\langle K|\ n_z\ |K-1\rangle = \langle K-1|\ n_z\ |\ K\rangle = \frac{1}{\sqrt{(4K^2-1)}} \qquad (2.17)$$

where Λ has been dropped. Let us now introduce spin and find the nonzero matrix elements in terms of M, J, S, and K. These are:[6]

$$\langle K\ S\ J\ M|\ n_z\ |K-1\ S\ J\ M\rangle = \langle K-1\ S\ J\ M|\ n_z|\ K\ S\ J\ M\rangle =$$

$$= \frac{M\sqrt{(J-S+K)(J+S+K+1)(S+K-J)(J+S-K+1)}}{2J(J+1)\sqrt{(4K^2-1)}}$$

$$\langle K\ S\ J\ M|\ n_z\ |K-1\ S\ J-1\ M\rangle = \langle K-1\ S\ J-1\ M|\ n_z\ |\ K\ S\ J\ M\rangle =$$

$$= \frac{\sqrt{(J^2-M^2)}\ \sqrt{(J-S+K)(J+S+K+1)(J-S+K-1)(J+S+K)}}{2J\sqrt{(4J^2-1)}\ \sqrt{(4K^2-1)}} \qquad (2.18)$$

It is understood that the initial and final states must be of opposite parity.

Coupling intermediate between Hund's case (a) and case (b)

As an example, intermediate coupling in the $^2\Pi$ electronic state will be discussed. Intermediate coupling in this situation can be described as a mixing of $^2\Pi_{1/2}$ and $^2\Pi_{3/2}$ rotational states having the same value of J. Corrections for intermediate coupling were made specifically in analysing the Stark effect on the $P_1(1)$ transition to the $J = 3/2$, $^2\Pi_{3/2}$ level in the OH molecule. The general result for this mixing can be written:[7]

$$(\psi_{int})_1 = a\psi(^2\Pi_{1/2}) \mp b\,\psi(^2\Pi_{3/2})$$
$$(\psi_{int})_2 = b\psi(^2\Pi_{1/2}) \pm a\,\psi(^2\Pi_{3/2}) \qquad (2.19)$$

$\psi(^2\Pi_{1/2})$ and $\psi(^2\Pi_{3/2})$ are pure Hund's case (a) wave functions. The upper signs in equations (2.19) are for regular doublets and the lower signs are for inverted doublets. The coefficients, a and b, in equations (2.19) are given by:[7]

$$a = \sqrt{\frac{X - 2 + (A/B)}{2X}}$$
$$b = \sqrt{\frac{X + 2 - (A/B)}{2X}} \qquad (2.20)$$

where $X = +\sqrt{4(J + \frac{1}{2})^2 + (A/B)(A/B-4)}$. (2.21)

A is the spin coupling constant and B is the rotational constant. For regular doublets A/B is positive and for inverted doublets A/B is negative. Hund's case (a) coupling corresponds to the ratio A/B becoming large. Specifically, as $A/B \to \infty$,

$a \rightarrow 1$ and $b \rightarrow 0$ and we see that:

$$(\psi_{int})_1 \rightarrow \psi(^2\Pi_{1/2}) \text{ and } (\psi_{int})_2 \rightarrow \psi(^2\Pi_{3/2});$$

as $A/B \rightarrow -\infty$, $a \rightarrow 0$ and $b \rightarrow 1$ and this corresponds to:

$$(\psi_{int})_1 \rightarrow \psi(^2\Pi_{3/2}) \text{ and } (\psi_{int})_2 \rightarrow \psi(^2\Pi_{1/2}).$$

It was convenient to use Hund's case (a) wave functions to treat intermediate coupling as the appropriate matrix elements are already available. The description given here may also be used to treat case (b) coupling by setting the coefficients given in equation (2.20): $a = b = 1/\sqrt{2}$. As a specific example, the expressions available here will be applied to an inverted $^2\Pi$ electronic state to evaluate the perturbation matrix elements for a lambda doublet rotational level in the $^2\Pi_{3/2}$ state. The appropriate wave function from equation (2.19) is:

$$(\psi_{int})_1 = a\psi(^2\Pi_{1/2}) + b\psi(^2\Pi_{3/2}) \qquad (2.22)$$

and the perturbation matrix element given in equation (2.12) become:

$$V_{12} = -\mu E\left\langle a\psi_{\pm}^*(^2\Pi_{1/2}) + b\psi_{\pm}^*(^2\Pi_{3/2}) \middle| \; n_z \; \middle| \; a\psi_{\mp}(^2\Pi_{1/2}) + b\psi_{\mp}(^2\Pi_{3/2}) \right\rangle \qquad (2.23)$$

The subscript $\pm$ indicates the parity of the initial and final state. As we have noted above, the combinations in equation (2.23) must obey the selection rule, $\Delta\Sigma = 0$. Thus equation (2.23) reduces to:

$$V_{12} = -\mu E\left[a^2\left\langle \psi_{\pm}^*(^2\Pi_{1/2}) \middle| \; n_z \; \middle| \; \psi_{\mp}(^2\Pi_{1/2}) \right\rangle + b^2\left\langle \psi_{\pm}^*(^2\Pi_{3/2}) \middle| \; n_z \; \middle| \; \psi_{\mp}(^2\Pi_{3/2}) \right\rangle\right]. \qquad (2.24)$$

This expression can be evaluated for a specific rotational level using expressions (2.15) and (2.20).

There are two topics remaining in this chapter. The Stark effect on spectra resulting from transitions between rotational levels which are both degenerate will be discussed, using the specific example of the CH $^2\Delta - ^2\Pi$ band. Leading to this the mixing of lambda doublet levels will be reviewed. The final topic for discussion will be second order Stark effects due to the interaction of neighboring rotational levels.

Parity mixing and transitions between perturbed lambda doublets

In describing a perturbed lambda doublet of mixed parity let us call the lower unperturbed level "1" (one) and the upper unperturbed level "2" and label the corresponding unperturbed eigen-functions as ψ_1 and ψ_2. The perturbed levels will be described by the eigen-functions:[8]

$$\psi_{low} = a\psi_1 + b\psi_2$$
$$\psi_{upp} = b\psi_1 - a\psi_2 \qquad (2.25)$$

where the coefficients a and b are given by:[8]

$$a = \sqrt{\frac{1}{2} + \frac{(\lambda/2)}{2\sqrt{(\lambda/2)^2 + (V_{12})^2}}}$$

$$b = \frac{V_{12}}{|V_{12}|}\sqrt{\frac{1}{2} - \frac{(\lambda/2)}{2\sqrt{(\lambda/2)^2 + (V_{12})^2}}} \qquad (2.26)$$

λ is the separation of the unperturbed lambda doublet levels and V_{12} is the matrix element for the perturbation energy.

The sign of the perturbation appearing in equation (2.26) will allow us to determine the relative sign of the electric dipole moment of the CH molecule in the initial and final state

from observations of the Stark effect on the $^2\Delta - ^2\Pi$ band. The perturbation contains the electric dipole moment whose direction is fixed relative to the internuclear axis of the molecule. The relative direction of the dipole moment will determine the relative sign of the perturbation which in turn will determine whether the coefficients a and b are positive or negative. If the relative splittings of the Stark components levels in the upper and lower state are known, the observed Stark spectra allows one to deduce whether the coefficient a or b of one state has the same or opposite sign as that in the other state. Thus we are able to deduce the relative sign of the dipole moments in the two states.

The transitions between two lambda doublet levels are shown in Figure 2.4 for zero electric field and in the presence of an electric field for the same and opposite relative signs of the dipole moment in the upper and lower state. (This example is general enough to be used later in discussing the perturbation between neighboring rotational levels.) The allowed transitions in Figure 2.4 are labelled I and II. The primes on the transitions in the presence of the field indicate forbidden transitions. If the dipole moments have the same relative sign the strong component of the lower frequency allowed line moves to higher frequency and the strong component of the higher frequency allowed line moves to lower frequency. (This conclusion assumes there are greater Stark shifts in the upper state than the lower state which is correct for the CH molecule.) If the relative signs of the dipole moment are opposite in the up-

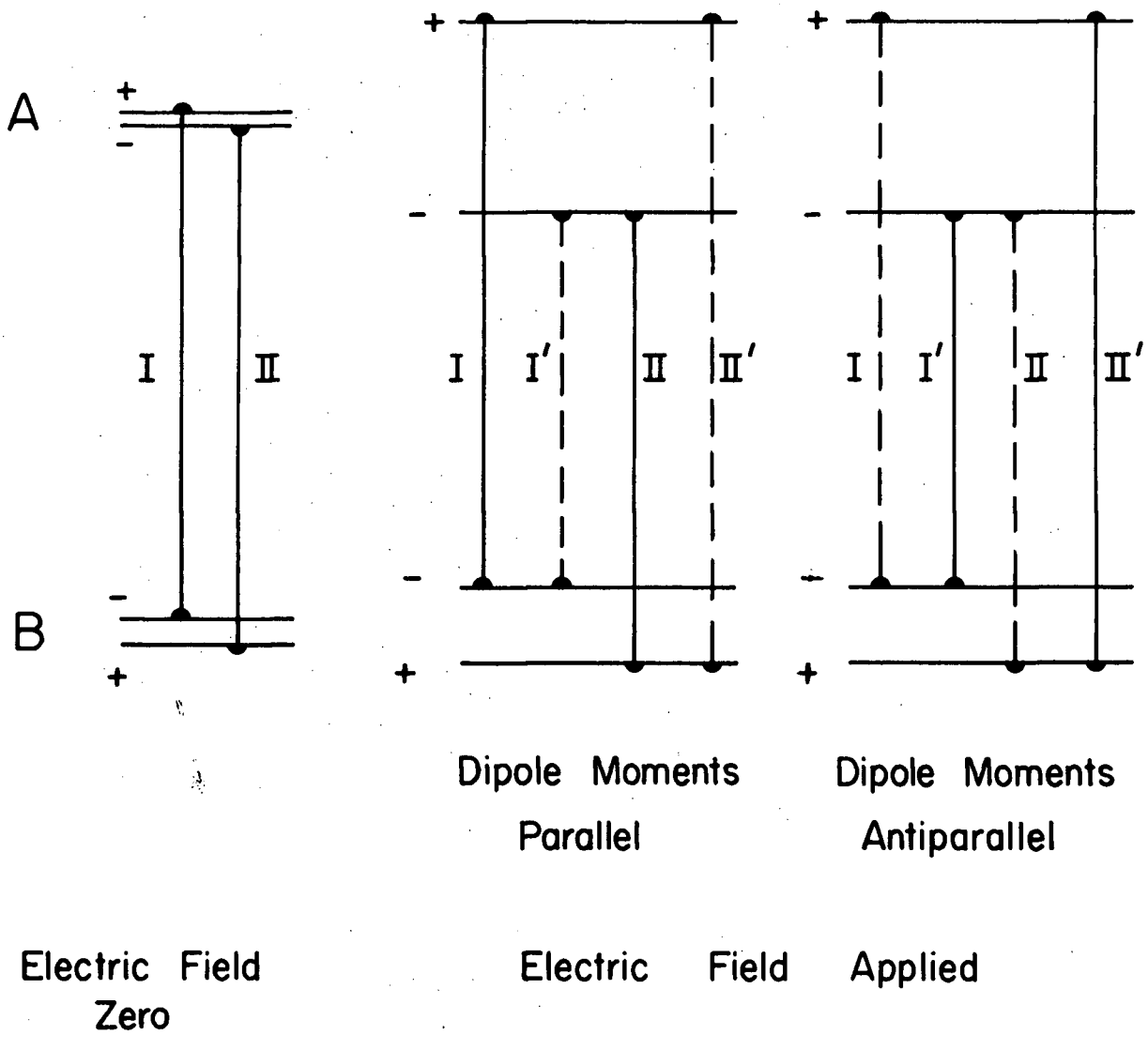

Figure 2.4. Zero field and field-induced, parity-forbidden transitions between lambda doublets. Broken lines indicate transitions with lower intensity.

per and lower states the strong Stark components move apart.

The intensities of the Stark transitions shown in Figure 2.4 can be given in detail by finding the perturbed wave functions. If the states have parity as shown in the figure and the relative dipole moments are the same in the levels marked A and B the wave functions are:

$$\begin{aligned} \text{A:}\ \psi_{low} &= +a_A\psi_+ + b_A\psi_- \\ \psi_{upp} &= +b_A\psi_+ - a_A\psi_- \\ \text{B:}\ \psi_{low} &= +a_B\psi_- + b_B\psi_+ \\ \psi_{upp} &= b_B\psi_- - a_B\psi_+ \end{aligned} \tag{2.27}$$

The transitions labelled I, I', II, and II' will have intensities proportional to:

$$\begin{aligned} \text{I:}\ & (a_Aa_B + b_Ab_B)^2 \\ \text{I}'\text{:}\ & (a_Ab_B - b_Aa_B)^2 \\ \text{II:}\ & (a_Aa_B + b_Ab_B)^2 \\ \text{II}'\text{:}\ & (-a_Ab_B + b_Aa_B)^2 \end{aligned} \tag{2.28}$$

We expect that a_A and b_A will be comparable to a_B and b_B respectively. Thus, we see when the dipole moments in the two states have the same relative sign the transitions labelled I and II will be strong and the forbidden transitions I' and II' will be weak. A similar argument can be made assuming the relative signs of the dipole moments in the initial and final state are opposite. This is equivalent to reversing the sign of the b coefficient in the description of one of the states and results in the reversing of the primes shown in equation (2.28). Thus if the relative signs of the dipole moment in the two states are

opposite the strong components move apart.

Figure 2.5 shows the Stark transitions for the $Q_{1c}(3)$ and $Q_{1d}(3)$ lines in the CH $^2\Delta - ^2\Pi$ band. The observed Stark effect showed the lines moving together as indicated in the figure. (Only the strong transitions are indicated.) The splittings were computed using a value of 1.0 Debye for the dipole moment of the $^2\Delta$ state and 1.46 Debye for the $^2\Pi$ state and a value of 66kV/cm for the electric field strength. The lambda doubling in the $^2\Delta$ state is effectively zero[9] and the lambda doubling in state was taken as 0.38 cm^{-1}. The figure shows that relative to the $Q_{1c}(3)$ line, for example, the greatest increase in frequency occurs for the M = 7/2 → M = 5/2 component.

Second order Stark effects

This final section will discuss contributions to second order Stark effects due to the interaction of neighboring rotational levels. The discussion is based on the expression for the second order correction in energy, ϵ^2, given by:[8]

$$\epsilon^2 = \sum_m{}' \frac{|V_{mn}|^2}{E_n - E_m} \qquad (2.29)$$

This is the correction for the level "n". The prime indicates the term for m = n is to be omitted from the sum. E_n and E_m are unperturbed values for the energies of the perturbing levels and V_{mn} is the matrix element for the perturbation energy between the levels "n" and "m". The matrix elements to be used in this equation are those given above and we recall that they are nonzero only between states of opposite parity and for

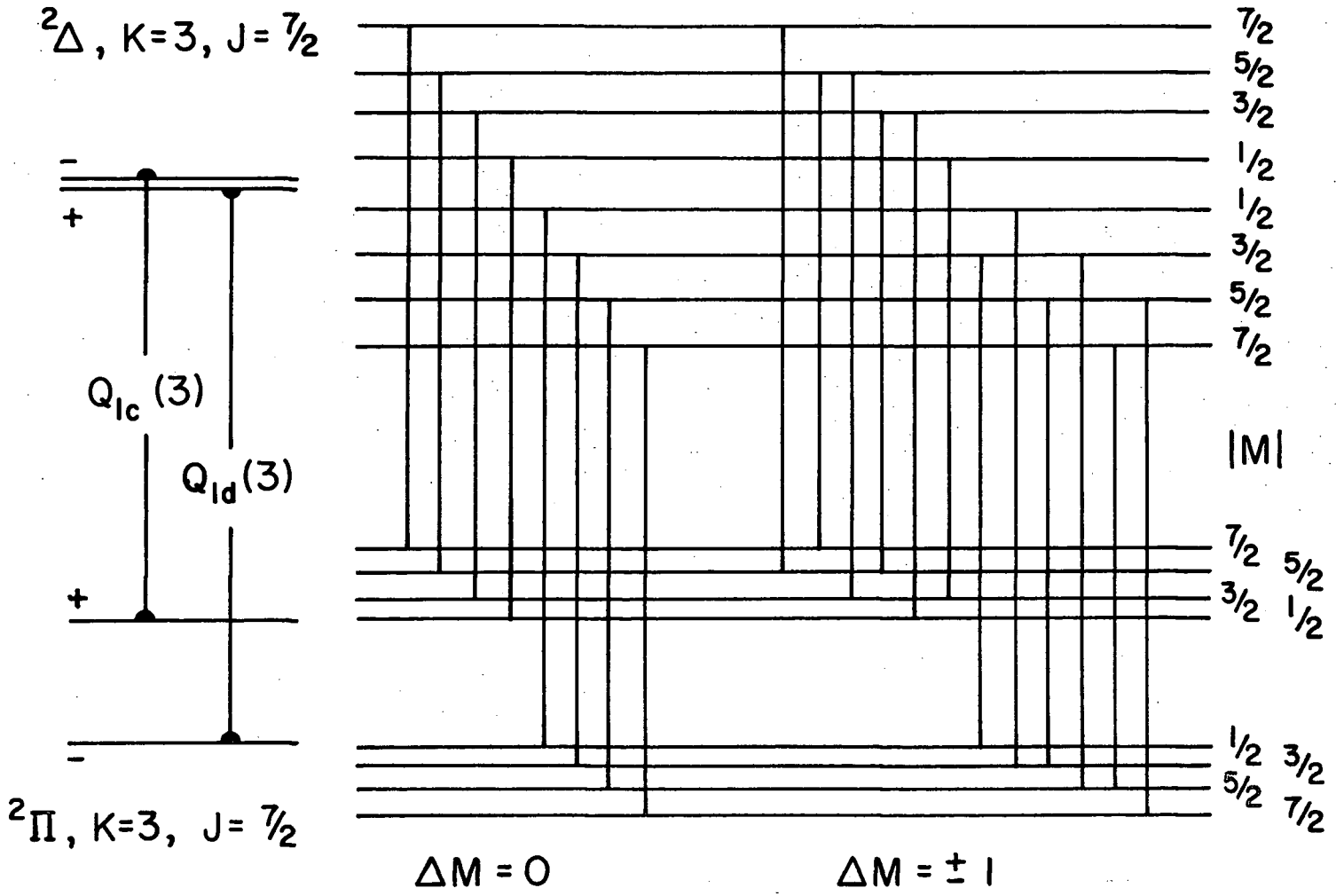

Figure 2.5. Stark effect on CH, $Q_{1c}(3)$ and $Q_{1d}(3)$ lines. Only strong Stark transitions are shown.

$\Delta J = \pm 1, 0$. Because of these restrictions on the matrix elements we need consider only the effects of neighboring rotational levels. To evaluate such effects in the $^2\Sigma$ state the matrix elements for Hund's case (b) coupling which are given in equations (2.17) and (2.18) can be applied immediately to equation (2.29).

For $^2\Pi$ states, the discussion of parity mixing in lambda doublets and transitions between them may be applied to greatly simplify the evaluation of second order corrections given by equation (2.29). Consider the situation shown in Figure 2.4, where the lambda doublet levels now belong to the same electronic and vibrational state and differ by one in J. It is sufficiently accurate for our purpose to take the separation between a lambda doublet level of one rotational state and either lambda doublet level of the other state as the mean separation of the rotational levels. The parity mixing of lambda doublets for the same rotational level is given by equations (2.25) and (2.26). Since the perturbation between rotational levels occurs between components with the same value of M one need find the parity mixing in the two lambda doublets for only one value of $|M|$ at a time.

The second order effect due to neighboring rotational levels will move both lambda doublet levels by the same amount. One can see that they move together from equations (2.29) and (2.28). A mixed lambda doublet component of one rotational level will be perturbed by both mixed lambda doublets of the other level. The energy difference in the numerator of equation

(2.29) is essentially the same for the transitions. From equation (2.29) we also see that the matrix elements are squared. The expressions in (2.28) show these squared matrix elements to within a factor. The expressions labelled I and I' sum to one (as do II and II'). The factor of proportionality for the expressions in (2.28) is the square of the matrix element for μEn_z between a rotational level of one parity and the adjacent level of opposite parity. Thus jointly, both lambda doublets of one rotational level push each lambda doublet component of the other rotational level by the same amount.

If the rotational levels correspond to coupling intermediate between Hund's case (a) and case (b) equations (2.20) and (2.24) can be applied. Pure Hund's case (b) can be treated as an equal mixture of pure Hund's case (a) wave functions.

Footnotes for Chapter II

1. G. Herzberg, Molecular Spectra and Molecular Structure. I. Spectra of Diatomic Molecules (D. Van Nostrand Co., New York, 1950), Second Edition, p. 300.

2. L. D. Landau and E. M. Lifschitz, Quantum Mechanics--Non-relativistic Theory (Addison-Wesley Publishing Co., Reading, Massachusetts, 1958), p. 203.

3. Herzberg, p. 240-244.

4. Landau and Lifschitz, p. 294-298.

5. Landau and Lifschitz, p. 295.

6. Landau and Lifschitz, p. 294-298 and p. 104-105.

7. G. C. Dousmanis, T. M. Saunders and C. H. Townes, Phys. Rev. 100, 1735 (1955).

8. Landau and Lifschitz, p. 139.

9. A. E. Douglas and G. A. Elliott, Can. J. Phys. 43, 496 (1965).

CHAPTER III

EXPERIMENTAL DETAILS

The Stark effect on the electronic emission spectra of diatomic molecules reported here was produced in an electric discharge tube similar to that used by LoSurdo. The electric field in the cathode dark space of such a low pressure discharge tube produces the Stark effect. (In the cathode dark space there is a high density of slow moving positive ions which produce a large drop in potential in a small distance with the resulting large electric field.[1]) The discharge tube not only provided the electric field but also supplied the desired molecule in an electronic excited state. The resulting Stark effect spectra were observed photographically. This chapter will discuss the experimental equipment and techniques used to produce the electric field and the electronically excited molecules. The observation of the Stark spectra and the determination of the electric field will also be discussed.

Electric discharge tube

Figure 3.1 shows a diagram of the discharge tube used in this study. The tube was blown from pyrex glass. The plane window and capillary tube insulating the cathode were both quartz. The window was sealed to the tube and the cathode was sealed in the quartz capillary using deKhotinsky cement. Often the rubber stopper was sealed using an "O" ring formed from Apiezon "Q" compound. The outlet of the discharge tube was con-

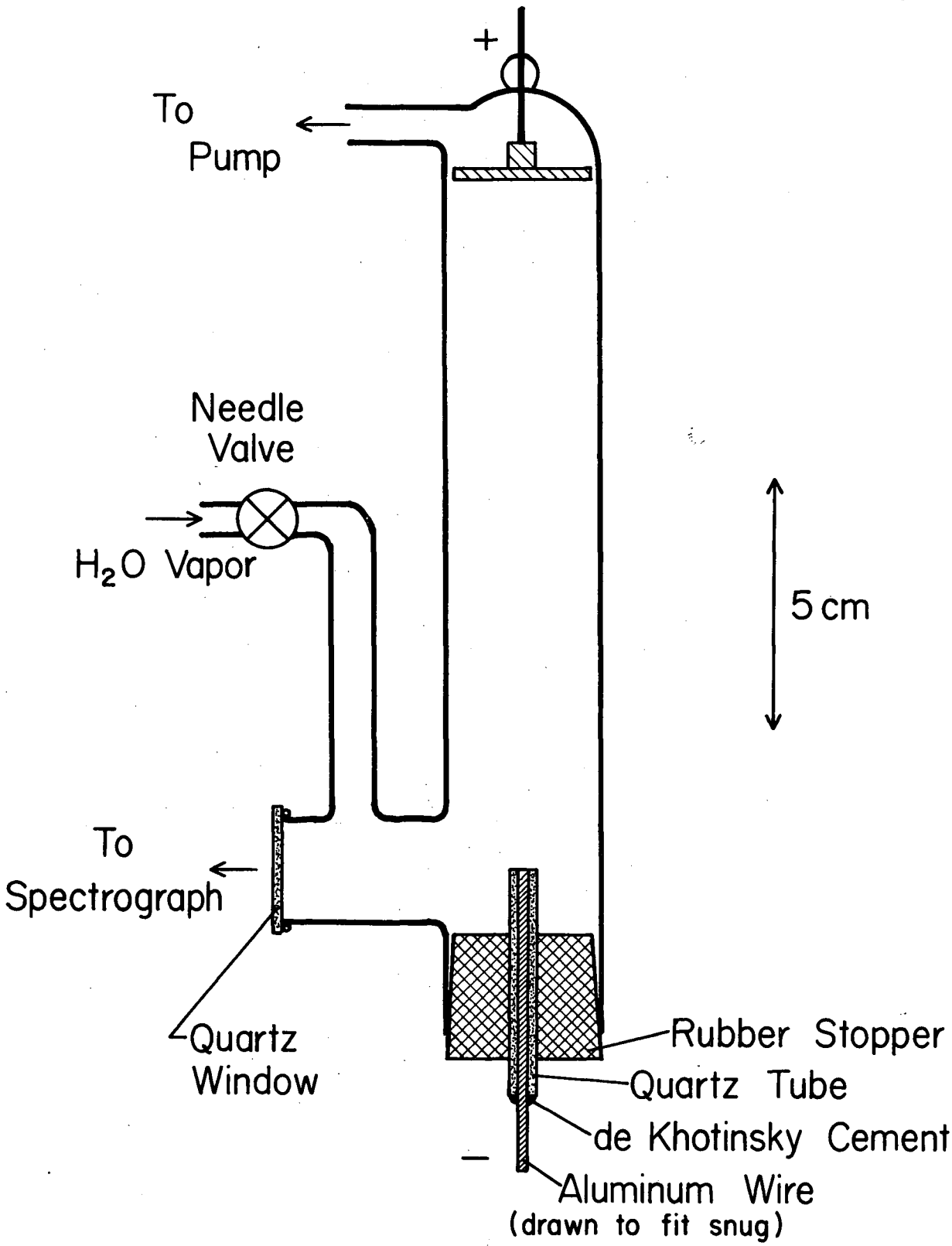

Figure 3.1. Modified Lo Surdo discharge tube.

nected to a mechanical pump via a liquid nitrogen trap. The pressure in the tube was measured with a McLeod guage located between the discharge tube and the cold trap. The diagram indicates the direction in which gas flowed while using H_2O vapour to produce OH molecules. (The gas inlet and pump connections were reversed for another application of the tube and remained that way when methyl alcohol vapour was used to produce CH molecules.) The direction of gas flow did not apparently alter the operation of the discharge. When using carbon compounds to produce CH molecules a liner was placed inside the discharge tube. In this way the tube walls could be quickly and easily cleaned when visual observation of the discharge became difficult. The liner was a pyrex glass cylinder fitting easily inside the discharge tube. The portion of the liner in front of the side tube leading to the quartz window was removed.

The discharge tube was operated as a direct current glow. Under these conditions most of the potential difference between the cathode and anode appears across the cathode dark space. For representative operating conditions of 4 kV across the discharge tube and 1 mm Hg total pressure the dark space would be about 1 mm and an electric field of about 40 kV/cm would be produced. The disc anode was made of aluminum and the electrical connection was via a tungsten wire-glass bead seal. The cathode was a wire, usually 1 mm diameter aluminum. The wire was sealed in a quartz tube so that only the end was exposed inside the tube. The upper end of the cathode was usually ground flat and flush with the end of the quartz tube. (A more detailed discus-

sion of cathode materials in various sizes appears below.) The anode (and positive terminal of the power supply) were grounded. Otherwise, the discharge would also go to ground via the pump. A ballast resistor of 50,000 ohms was placed in series with the discharge tube to limit the current.

Basic operating procedure was determined by factors affecting the short term stability and the useful lifetime of the cathode. Short term stability was limited by the ability of the cathode to dissipate heat. Too much power would destroy the useful portion of the cathode immediately. The useful lifetime of the cathode was limited by sputtering which lowered the cathode surface (and the high field region) into the quartz tube. Since the inside walls of the quartz tube were covered with opaque sputtered material the high field region disappeared from view after a few hours at most.

The discharge was started at relatively low voltages and currents and run until a small pit was burned in the center of the cathode surface. A bright cone in the discharge extending from the pit into the positive column would appear almost immediately. When the bright cone would remain stable and narrow for increased voltages the applied voltage could be raised to some chosen value and the pressure increased until the current corresponded to the maximum safe power. (The power dissipated in the whole tube was generally limited to about 20 watts to insure stable operation.) Alternatively, when the discharge first became stable a pressure could be chosen and then the voltage increased.

Production of OH and CH electronic emission spectra

Relatively strong and pure ultraviolet OH emission spectra were observed when H_2O vapour was used in the discharge tube. The vapour was supplied from a trap containing carefully degassed liquid H_2O and connected to the discharge tube via a needle valve. The vapour was continuously flowed through the discharge tube. The pressure of H_2O vapour in the discharge tube ranged from 0.5 to 4.0 mm Hg. The pressure was set by adjusting the flow rate through the needle valve. Variations in pressure due to changes in the temperature of the liquid H_2O were reduced by using a water bath or by pumping on the liquid until an equilibrium temperature was reached.

Experiments were done with aluminum cathodes 2.0, 1.0, and 0.5 mm in diameter and with a tungsten cathode 1.0 mm in diameter. The largest cathodes were difficult to use as local heating on the cathode surface often became excessive and the central pit was destroyed. Tungsten was even more difficult to use as it would often evaporate from the cathode surface and coat the quartz tube insulating the cathode. The evaporated coating conducted electrically and caused the character of the discharge to change completely. The 1.0 mm diameter aluminum cathode was the easiest to use and produced electric fields up to 60 kV/cm. The largest electric field in the study of the OH molecule, 63 kV/cm, was produced using the 0.5 mm diameter aluminum cathode. However, these small cathodes were difficult to use and often melted when the discharge was first started. In the study of the OH molecule the voltage across and current through the

discharge tube ranged from about 3.6 kV and 12 ma for 2 mm diameter cathodes to about 6.5 kV and 4.2 ma for 1 mm cathodes and about 3 kV and 2.4 ma for 0.5 mm cathodes.

Electronic emission spectra from the CH molecule were produced in the discharge tube using methyl alcohol vapour. Helium or H_2 was sometimes used as a carrier gas. The best combination was CH_3OH vapour and He gas with a partial pressure of 0.2 to 0.4 mm Hg for the vapour and a total pressure of 1 to 3 mm Hg. The use of H_2 as a carrier gas was not very satisfactory even though it sometimes enhanced the intensity of atomic hydrogen Balmer lines which were used to determine the electric field strength. The resulting H_2 molecular lines complicated the problem of identifying and studying a chosen CH molecular line. For the preliminary study of CH emission spectra the carrier gas when used flowed over alcohol contained in a trap. The most satisfactory arrangement, however, was to introduce the alcohol vapour and carrier gas through separate needle valves. In this way the pressure of the two gasses could be set easily and independently. When CH_3OH vapour and He were used the relative intensity of the atomic hydrogen Balmer line, H_γ and the helium line at λ6678Å was observed visually. These observations were made through the side of the discharge with a prism spectroscope and very much aided the adjustment of discharge conditions before observing the molecular spectra. In fact, from such visual observations it was possible to roughly estimate the electric field strength.

The use of a hydrocarbon such as methane, propane, benzene

or cyclohexane did not prove satisfactory for the production of CH emission spectra either when used alone, with the addition of a carrier gas or when mixed with alcohol with or without the addition of a carrier gas. Such substances in the discharge tube produced an electrically conducting deposit on the cathode surface which quickly destroyed the stability of the discharge.

For studying the Stark effect on the spectra of the CH molecule, 1 mm diameter aluminum cathodes were generally used. Applied voltages ranged from 3.0 to 5.0 kV and currents ranged from 3.0 to 6.7 ma. When studying the Stark effect on the OH and CH molecules simultaneously CH_3OH vapour and He gas was used in the discharge tube and the experimental conditions were essentially as described above except that the power dissipated in the discharge tube was kept at 15 watts or less.

Observing the Stark effect

The Stark effect was observed by focusing the light from the region of high electric field onto the slit of a stigmatic spectrograph and photographing the spectra. (The high electric field is in the cathode dark space. The electric field is zero at the cathode surface and almost zero again a millimeter or two above the cathode surface.) For the study of OH molecular spectra and the preliminary study of CH molecular spectra, a pair of plano convex quartz lens having a combined focal length of about 15 cm was used. For the simultaneous study of OH and CH molecular spectra, a pair of quartz-water achromatic lens with a combined focal length of about 18 cm was used. The molecular

Stark spectra were photographed with a 3.4 meter Ebert spectrograph equipped with a 30,000 line per inch grating. The OH band λ3064Å was photographed in fourth order with a resulting plate dispersion of 4.2 cm^{-1}/mm (0.39 Å/mm). The CH band λ3900Å was photographed in second order with a dispersion of 7.4 cm^{-1}/mm (0.83 Å/mm). When these OH and CH bands were observed simultaneously the OH band was again photographed in fourth order and the CH band was photographed in third order with a plate dispersion of 4.0 cm^{-1}/mm (0.61 Å/mm). The CH λ4300Å band was photographed in third order with a dispersion of 2.8 cm^{-1}/mm (0.51 Å/mm). Kodak 103a-0 plates were used for all photographs. Exposure times were usually about two hours. Plates were developed as recommended by the Eastman Kodak Company.[2]

Determination of the electric field strength

In order to determine the electric dipole moment of a molecule from the observed Stark splittings in the spectra one must know the corresponding electric field strength. For the study of the OH Stark spectra and the preliminary study of CH Stark spectra the electric field strength was determined from the Stark effect on atomic hydrogen Balmer lines. The Stark splittings of the atomic hydrogen Balmer lines were chosen because of the large observed shifts in frequency, typically 40 to 60 cm^{-1} on either side of the undisplaced line. Also the Stark effect in hydrogen has been studied extensively and results obtained experimentally and theoretically agree very well. The relation between the applied electric field and the observed

Stark splittings are known to terms in the third power of the applied field. (See for example, Condon and Shortley, The Theory of Atomic Spectra, p. 397.)[3]

The hydrogen Stark splittings and molecular Stark spectra were photographed simultaneously with the same spectrograph. In this way drifts, in the electric field and in the molecular Stark splittings, if present, were averaged in the same way. (During the study of OH spectra, hydrogen Stark splittings were sometimes also observed through the wall of the discharge tube and photographed with a Hilger medium quartz spectrograph. However, in only one case was it necessary to use a value for the electric field determined by this means. Comparisons in other experiments showed that fields determined from prism and grating photographs agreed to within 1%.)

When the Stark spectra of the CH λ3900Å band was observed in third order it was not possible to simultaneously observe the Stark splitting of a hydrogen Balmer line. For this reason OH Stark spectra and CH Stark spectra were observed simultaneously using one spectrograph and the electric dipole moment of the CH molecule was determined relative to that of the OH molecule.

Footnotes for Chapter III

1. For a discussion of low pressure glow discharges see for example: F. A. Maxwell and R. R. Benedict, Theory of Gaseous Conduction and Electronics (McGraw Hill Book Co., New York, 1941), pp. 311-325; or J. D. Cobine, Gaseous Conductors, (Dover Publications, New York, 1958), pp. 212-216.

2. Developing procedure used is given in:
Kodak Plates and Films for Science and Industry, Data Book P-9 (Eastman Kodak Co., Rochester, New York, 1962).

3. E. U. Condon and G. H. Shortley, The Theory of Atomic Spectra (Cambridge University Press, Cambridge, England, 1935) p. 397.

CHAPTER IV

EXPERIMENTAL OBSERVATIONS

The Stark effect on the electronic emission spectra of the OH and CH molecules was studied for electric fields in the range: 35 kV/cm to 65 kV/cm. Specifically, the OH, $^2\Sigma^+ \rightarrow {}^2\Pi$, (0,0) and (1,1) band, the CH, $^2\Sigma^- \rightarrow {}^2\Pi$, (0,0) band and the CH, $^2\Delta \rightarrow {}^2\Pi$, (0,0) band were studied. (The electronic emission spectra and the electric field causing the Stark effect were produced by a low pressure direct current glow discharge tube.) From observations of the Stark effect on these electronic emission spectra the electric dipole moment was found in the OH, $^2\Pi$, ground electronic state, in the CH, $^2\Pi$, ground electronic state, and in the CH, $^2\Delta$, excited electronic state.

To facilitate discussion and comparison of the Stark on these emission spectra the similar aspects will be presented in the following order: 1) observations including representative spectrograms followed by a qualitative discussion of them, 2) measured values of the observed Stark splittings in OH and CH lines and the positions of OH field-induced, parity-forbidden lines observed in the (0,0) band, 3) an analysis of these data, and 4) the experimentally determined values for the electric dipole moment of OH and CH.

Stark effect on the OH, $^2\Sigma^+ \rightarrow {}^2\Pi$ band

To introduce the OH spectrograms, Figure 4.1 shows the allowed transitions to the lowest rotational level of the $^2\Pi_{1/2}$

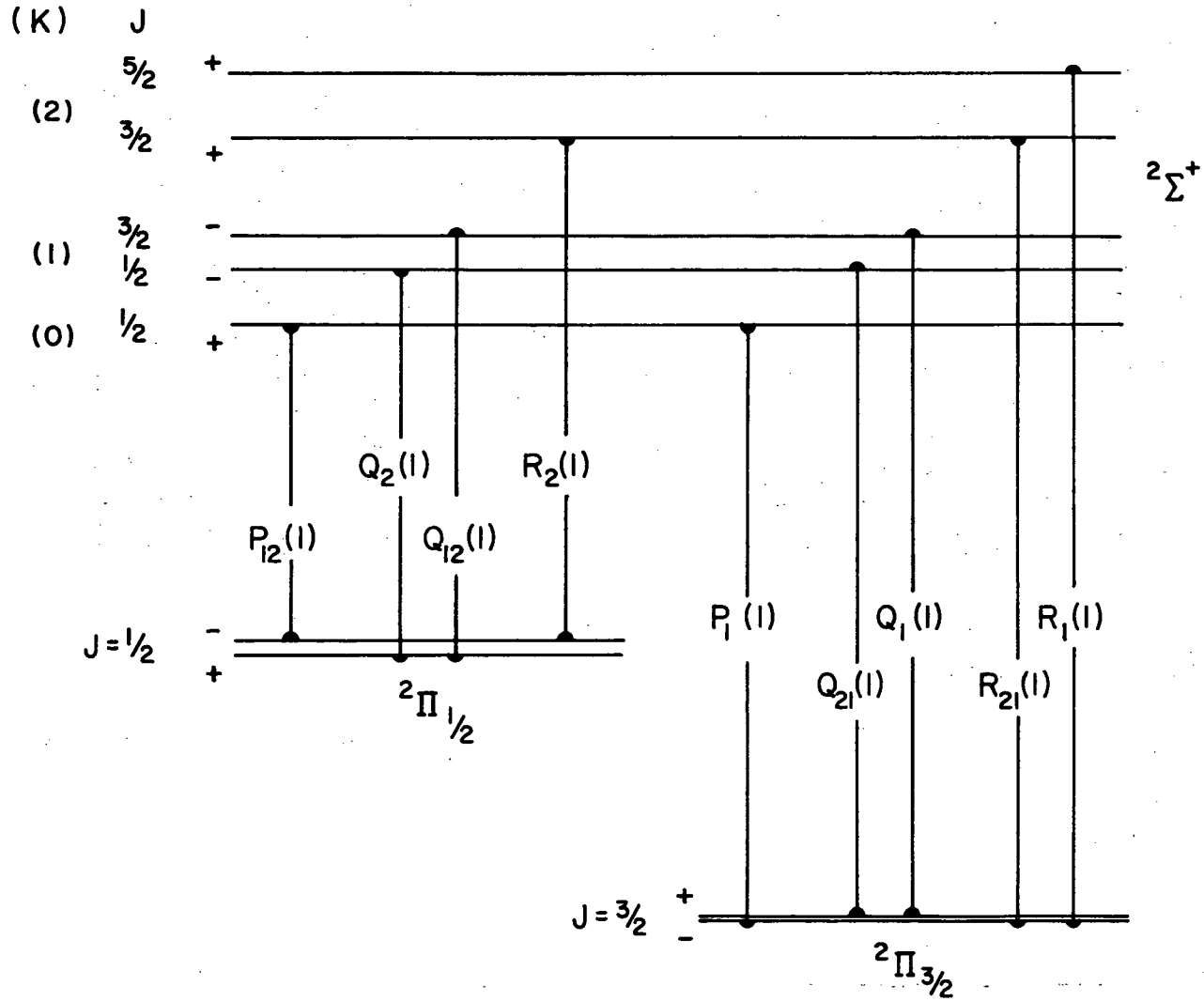

Figure 4.1. Allowed transitions to lowest rotational level in OH $^2\Pi_{1/2}$ and $^2\Pi_{3/2}$ states.

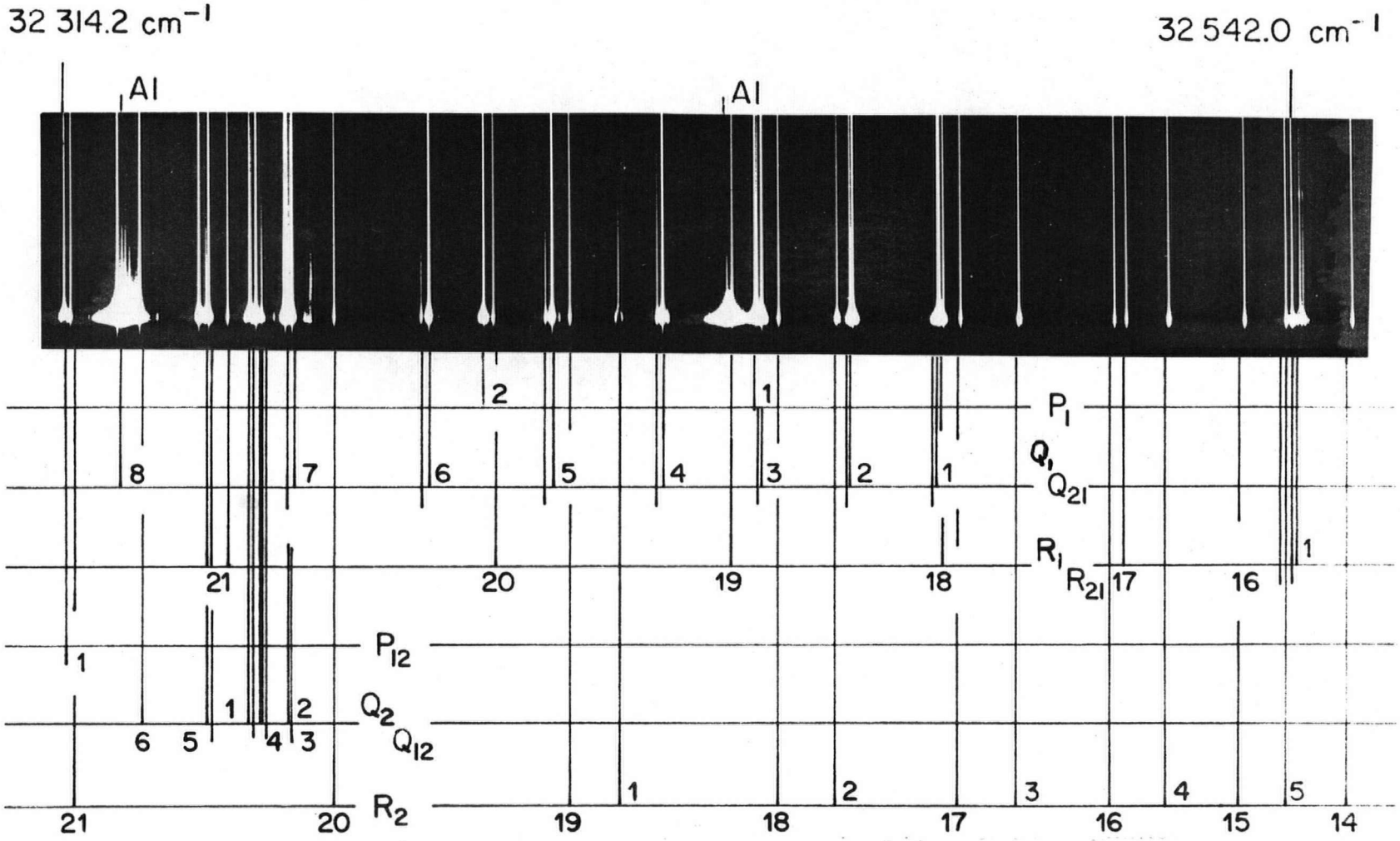

Figure 4.2. Stark effect on OH, $^2\Sigma^+ \rightarrow {}^2\pi$, (0,0) band. Maximum field region (63 kV/cm) is near bottom of print.

and $^2\Pi_{3/2}$ electronic states of the OH molecule. The figure includes the relevant rotational levels in the $^2\Sigma^+$ electronic state from which the transitions originate. (The diagram exaggerates the λ-type doubling in the $^2\Pi$ state and the spin doubling in the $^2\Sigma$ state.) With this diagram in mind let us now turn to Figure 4.2 which is an enlarged portion of a photographic plate and shows a portion of the OH, $^2\Sigma^+ \rightarrow {}^2\Pi$, (0,0) band, $\lambda 3064\text{Å}$. Wave number frequency increases to the right and the high field region is at the bottom of the lines. The maximum electric field is 63 kV/cm.

The simplest pattern of Stark splittings occur for transitions to the J = 1/2 level of the $^2\Pi_{1/2}$ state. These transitions are $P_{12}(1)$, $Q_2(1)$, $Q_{12}(1)$ and $R_2(1)$. For a J = 1/2 rotational level there is only one possible value of |M| for each lambda doublet level and the Stark effect will produce doublets. (This was shown in Figure 2.2 in Chapter II.) The expected doublets appear in the high field region for each of the appropriate lines. As seen from the energy level diagram in Figure 4.1, the $P_{12}(1)$ and $R_2(1)$ transitions terminate at the upper lambda doublet level of the J = 1/2, $^2\Pi_{1/2}$ state and as a result the forbidden components of the $P_{12}(1)$ and $R_2(1)$ appearing in the high field region are on the high frequency side of the respective allowed lines (to the right). We also see in the plate that the allowed components of the $P_{12}(1)$ and $R_2(1)$ lines shift to lower frequency in the high field region. Since the allowed $Q_2(1)$ and $Q_{12}(1)$ transitions go to the lower lambda doublet level, the positions of the forbidden and allowed components for these two

lines will be reversed relative to those of the $P_{12}(1)$ and $R_2(1)$ lines. (The slight separation of the $Q_2(1)$ and $Q_{21}(1)$ lines in the absence of the electric field is due to the spin splitting of 0.32 cm^{-1} [1] in upper rotational level, K = 1, $^2\Sigma^+$.)

The transitions to the J = 3/2 (the lowest) level of the $^2\Pi_{3/2}$ electronic state are $P_1(1)$, $Q_1(1)$, $Q_{21}(1)$, $R_1(1)$ and $R_{21}(1)$. Since the values of |M| can be 1/2 and 3/2 each lambda doublet level of the J = 3/2 level will yield two Stark components and a quartet will result. (See again Figure 2.2) The two low frequency components of the $P_1(1)$ line are visible beside the broad aluminum line on the left. The $Q_1(1)$ and $Q_{21}(1)$ lines each have Stark components with the same relative separation. However, for this plate the Stark pattern of one line falls midway between that of the other (because of spin splitting) and one sees only a very broad line. The $R_1(1)$ and $R_{21}(1)$ lines are more separated than the $Q_1(1)$ and $Q_{21}(1)$ lines due to a greater spin splitting, 0.47 cm^{-1}, [1] in the upper state ($^2\Sigma^+$, K = 2, J = 5/2, 7/2). As a result the three higher frequency Stark components of the $R_{21}(1)$ line fall on the three lower frequency components of the $R_1(1)$ line and the Stark components are clearly resolved. (The lowest frequency Stark component of the $R_{21}(1)$ line is blended and the highest frequency component of the $R_1(1)$ was very faint even on the original spectrographic plate.

Figure 4.2 clearly shows several field-induced, parity-forbidden lines completely separated from the associated allowed line. One also sees the decrease in Stark broadening with in-

creasing values of J. These features are related to the increasing number of Stark components with increasing values of J and the corresponding decrease in the separation of the Stark components and decrease in the effect of the perturbation on the lambda doublets. The lines $Q_1(1)$ to $Q_1(5)$ show these features. (When distinct forbidden lines appear the component associated with the Q_{21} line is overlapped by the allowed Q_1 line.) A reduction in Stark broadening with increasing J can also be seen in the lines, $R_2(1)$ to $R_2(4)$. However, in this example the forbidden components do not stand out separately because the lambda doubling in the $^2\Pi_{1/2}$ state decreases for the first few rotational levels and then increases for still higher values of J.[1]

Figure 4.3 shows an enlarged portion of Figure 4.2. (The maximum electric field is 63 kV/cm.) The two lines with forbidden lines on their right that are seen on either side of the $R_2(1)$ line are $Q_1(4)$ and $Q_1(5)$, from left to right. The broadening of the $P_1(2)$ line is very apparent. The print also shows the forbidden components for the $P_{12}(1)$, $Q_2(1)$, $Q_{12}(1)$, and $R_2(1)$ lines more clearly than above.

Figure 4.4 shows a portion of the OH, $^2\Sigma^+ \rightarrow {}^2\Pi$, (1,1) band. This plate was taken simultaneously with the previous two. The spectra are generally fainter but still clearly show resolved Stark splittings, e.g. the $P_{12}(1)$ line, Stark broadening, e.g. the $P_1(2)$ line, and field-induced, parity-forbidden lines, e.g. the line marked "F" on the left of the $P_1(2)$ line. The two broad lines that bend to lower frequencies are due to the N_2^+ molecule. (The cathode surface was tilted slightly to-

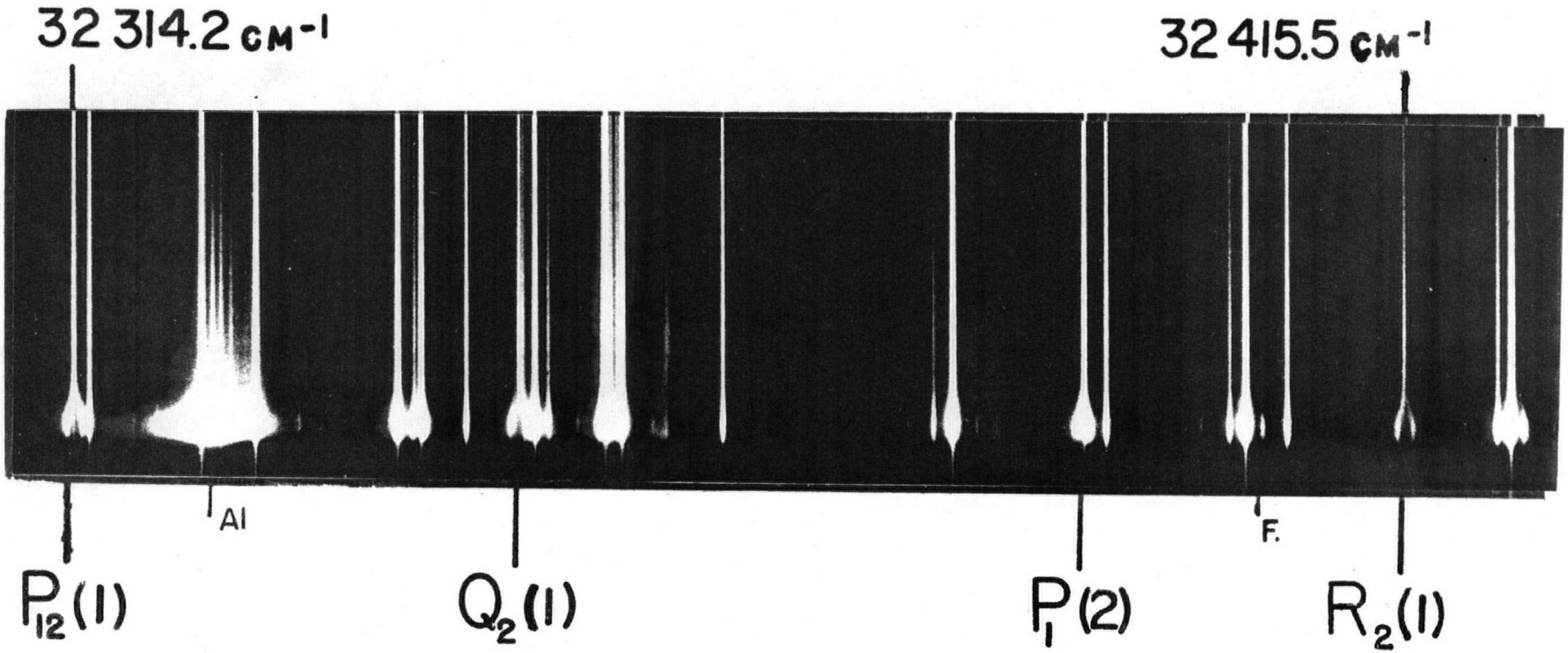

Figure 4.3. Stark effect on OH. Maximum field region is near bottom of print. (This is an enlargement of Figure 4.2, left half.)

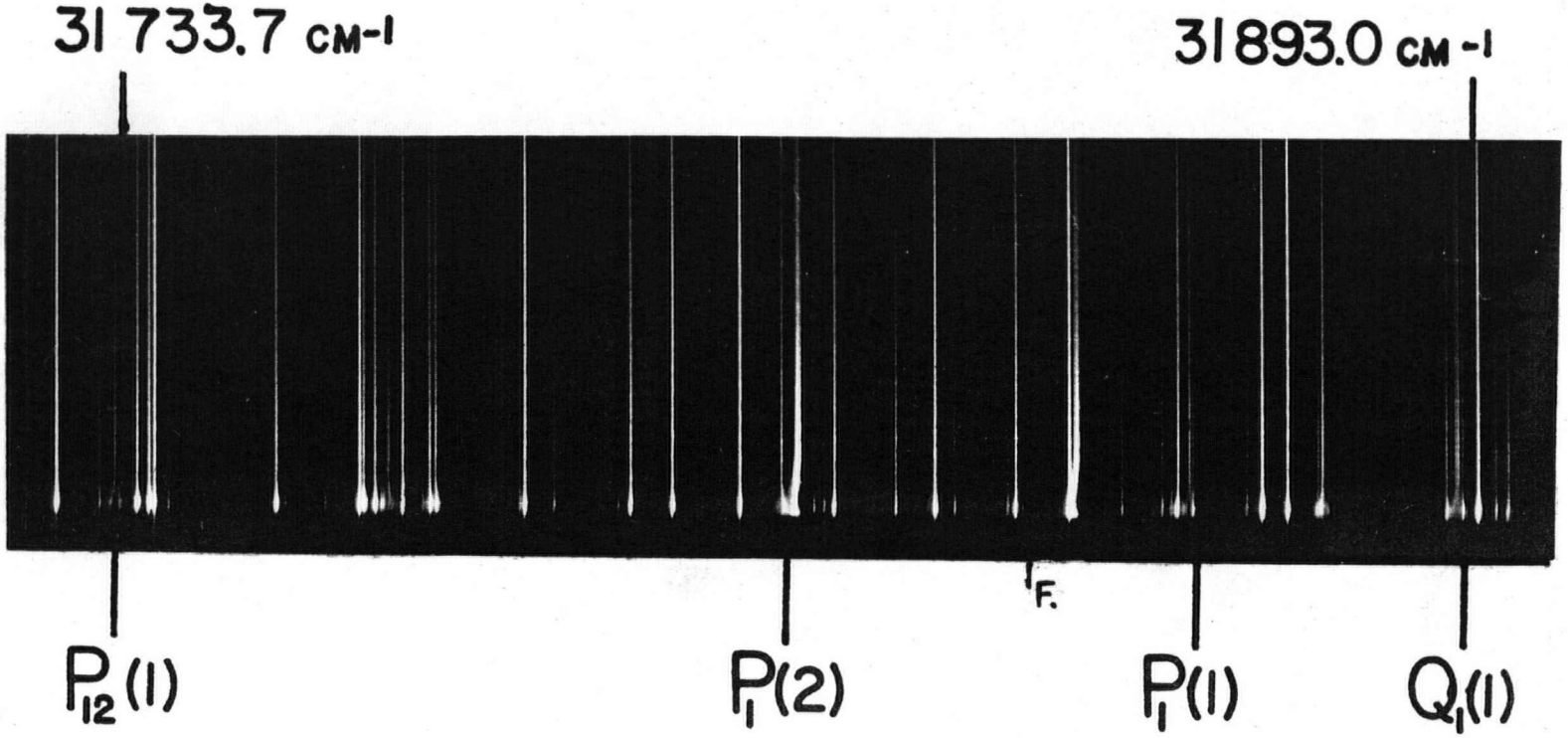

Figure 4.4. Stark effect on OH, $^2\Sigma^+ \rightarrow {}^2\Pi$, (1,1) band. Maximum field region (63kV/cm) is near bottom of print.

ward the slit and the Doppler shift resulted because the electric field moved the molecule.)

Stark effect on the CH, $^2\Sigma^- \rightarrow {}^2\Pi$ band

Figure 4.5 shows an enlarged portion of a spectrogram of the CH, $^2\Sigma^- \rightarrow {}^2\Pi$, (0,0) band, λ3900Å taken in third order. The electric field in the region of maximum splitting is about 52 kV/cm. The CH lines in Figure 4.5 are broad because of the rather high pressure in the discharge tube. Pecular discharge conditions caused the change of intensity in the lower portion of the lines; the unmarked lines are due to the N_2^+ molecule. Even so the plate clearly shows the numerous features due to the Stark effect on this CH band.

A review of Figure 4.1 which shows the energy levels of the OH molecule will aid the understanding of the CH spectra in the plate if the following points are taken into account: The upper state in the CH molecule from which the observed transitions originates is a $^2\Sigma^-$ state hence the relative position for an allowed and forbidden CH Stark component will be reversed from that observed in the OH spectra discussed above. See for example the OH, $R_2(1)$ line in Figure 4.3 and the CH, $R_2(1)$ line in Figure 4.5. The spin splitting in the CH $^2\Sigma^-$ electronic state is very small, less than 0.3 cm^{-1} [2] even when K = 5. Also the CH $^2\Pi$ electronic state belongs nearly to Hund's case (b) coupling for which the satellite lines are very weak. The other difference between the CH and OH molecule, although it does not alter the observed Stark effect, is that the $^2\Pi$ state

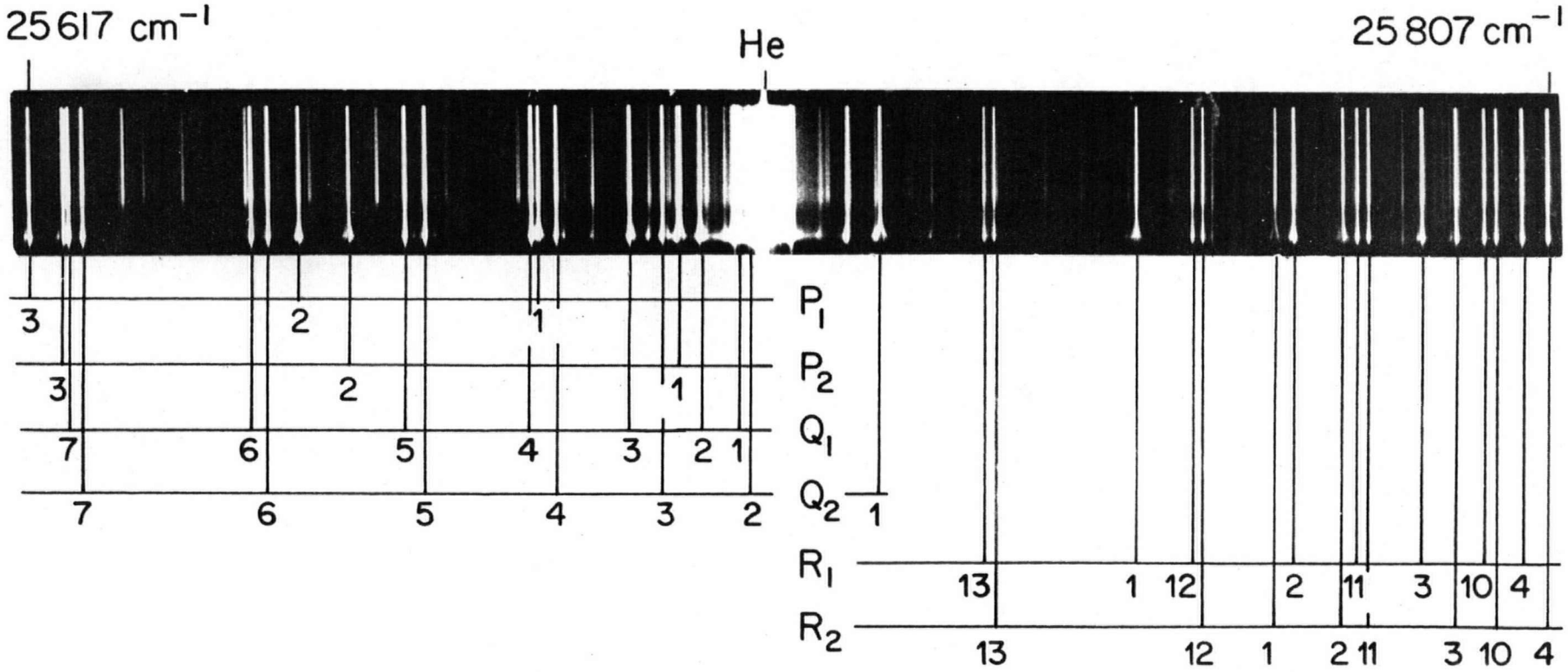

Figure 4.5. Stark effect on CH, $^2\Sigma^- \rightarrow {}^2\pi$, (0,0) band. Maximum field region (52 kV/cm) is near bottom of print.

in CH is regular while that in OH is inverted.

Figure 4.5 shows that the CH $P_2(1)$, $Q_2(1)$ and $R_2(1)$ lines resulting from transitions to the J = 1/2 level of the $^2\Pi_{1/2}$ state, are doublets in the high field region. The $R_1(1)$ line shows a splitting into four Stark components as expected for a transition to the J = 3/2 level of the $^2\Pi_{3/2}$ state. For this particular plate the $P_2(2)$ line showed four Stark components due to a transition to the J = 3/2 level of the $^2\Pi_{1/2}$ state. Also this plate shows very clearly the reduction in broadening and increase in separation of allowed and forbidden Stark components with increasing values of J. See for example the lines: $P_1(1)$ to $P_1(3)$, $P_2(1)$ to $P_2(3)$, $R_1(1)$ to $R_1(4)$, and $R_2(1)$ to $R_2(4)$. The relative location of the allowed and forbidden Stark components can be easily seen by comparing the $P_1(3)$, $Q_1(3)$, and $R_1(3)$ lines. Relative to the allowed line, the forbidden component is at lower frequencies for the P_1 and R_1 lines and at higher frequencies for the Q_1 line. The $Q_1(1)$ and $Q_2(1)$ lines obscured by the Helium line, λ3888.65Å, appear in the center of Figure 4.6 (b).

Figure 4.6 provides an opportunity to observe the Stark effect on the CH $^2\Sigma^- \rightarrow {}^2\Pi$ band for three different values of the electric field strength. The electric field increases going down the figure from (a) to (c). The electric fields are: (a) 34 kV/cm, (b) 47 kV/cm, and (c) 68 kV/cm. The increase in splitting with electric field shows most clearly for the $Q_2(1)$ line. These prints cover about the left three quarters of the previous plate (Figure 4.5) plus, from left to right, the $Q_1(8)$

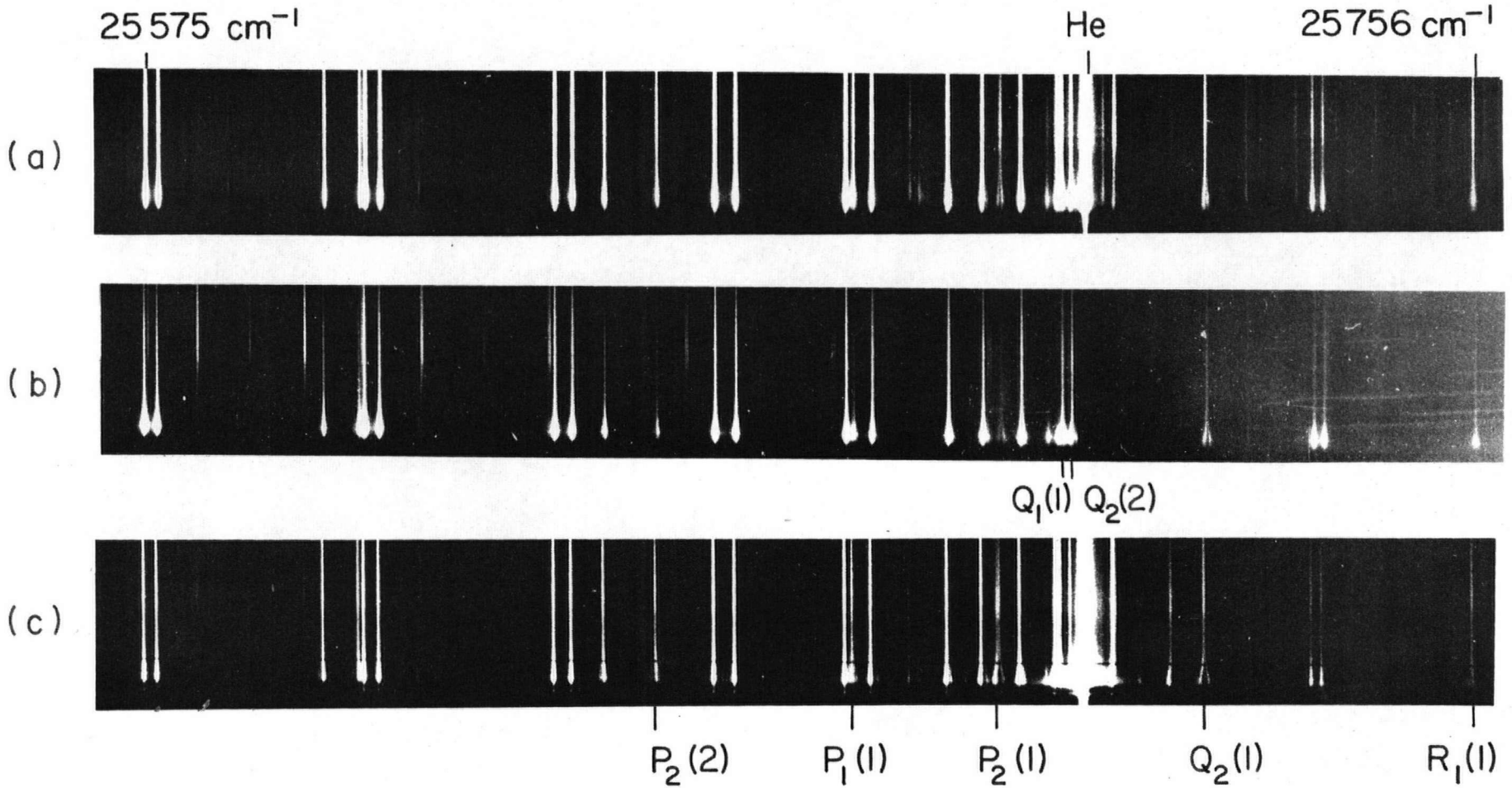

Figure 4.6. Stark effect on CH $^2\Sigma \rightarrow {}^2\Pi$, (0,0) band for three values of electric field. (a) 34 kV/cm, (b) 47 kV/cm, (c) 68 kV/cm. Maximum field region is near bottom of print.

and $Q_2(8)$ lines at the left edge of the prints. This series of plates also shows that the features related to the Stark effect become more pronounced as the electric field increases.

Stark splittings in the atomic hydrogen Balmer line H_γ

Figure 4.7 shows the Stark effect on the atomic hydrogen line H_γ, $\lambda 4340.47$Å. The maximum electric field is about 36 kV/cm and the splitting between the two 18π components is about 83 cm^{-1}. The photograph was taken in second order. (The discharge tube contained methyl alcohol vapour thus producing CH molecular lines. (The CH lines appearing on this print belong to the P branches of the $^2\Delta \rightarrow {}^2\pi$, (0,0) band.) The (b) part of Figure 4.7 shows the location of the Stark components of the H_γ line. The locations are drawn for an electric field of 36 kV/cm which corresponds to the maximum electric field on the print. The numbers 2,3,5, etc. in the drawing give the displacement of a given component in units of 0.0642 E cm^{-1}, where E is the magnitude of the electric field strength in kV/cm. (The relative intensities indicated in the drawing are from Condon and Shortley, The Theory of Atomic Spectra, page 401.)[3] The Stark splittings of the Balmer H_γ line were used to determine the electric field strength in the study of the Stark effect on OH emission spectra and in the preliminary study of the Stark effect on the CH emission spectra.

Stark effect on the CH $^2\Delta \rightarrow {}^2\pi$ band

Figure 4.8, the final spectrogram, shows the Stark effect

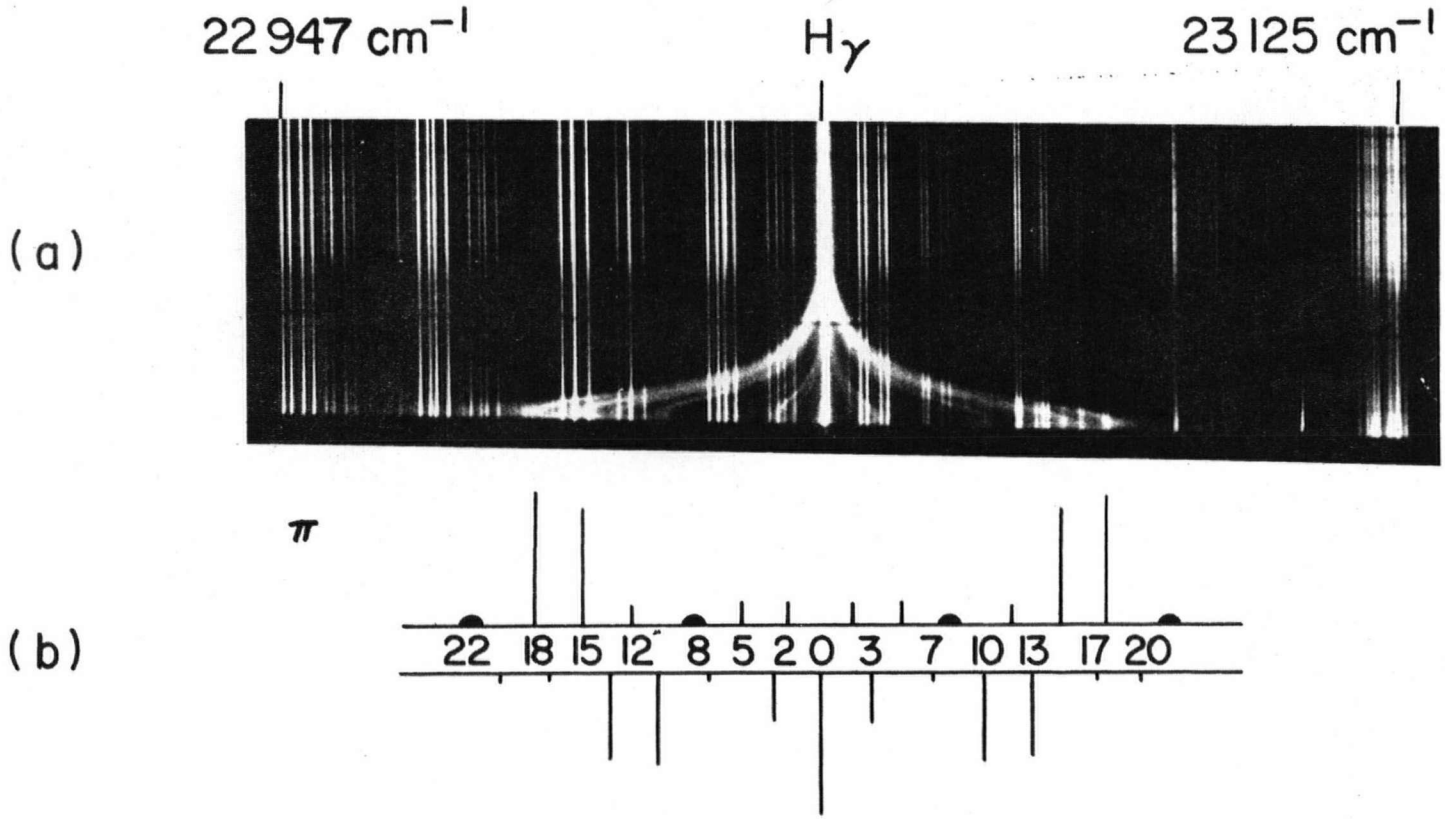

Figure 4.7. Stark effect on hydrogen Balmer H_γ. (a) Observed H_γ Stark splittings. Maximum electric field is 36 kV/cm. (Molecular lines are from CH $^2\Delta \rightarrow {}^2\pi$ band.) (b) Theoretical splittings and intensities. Splittings are drawn for 36 kV/cm (maximum field on plate).

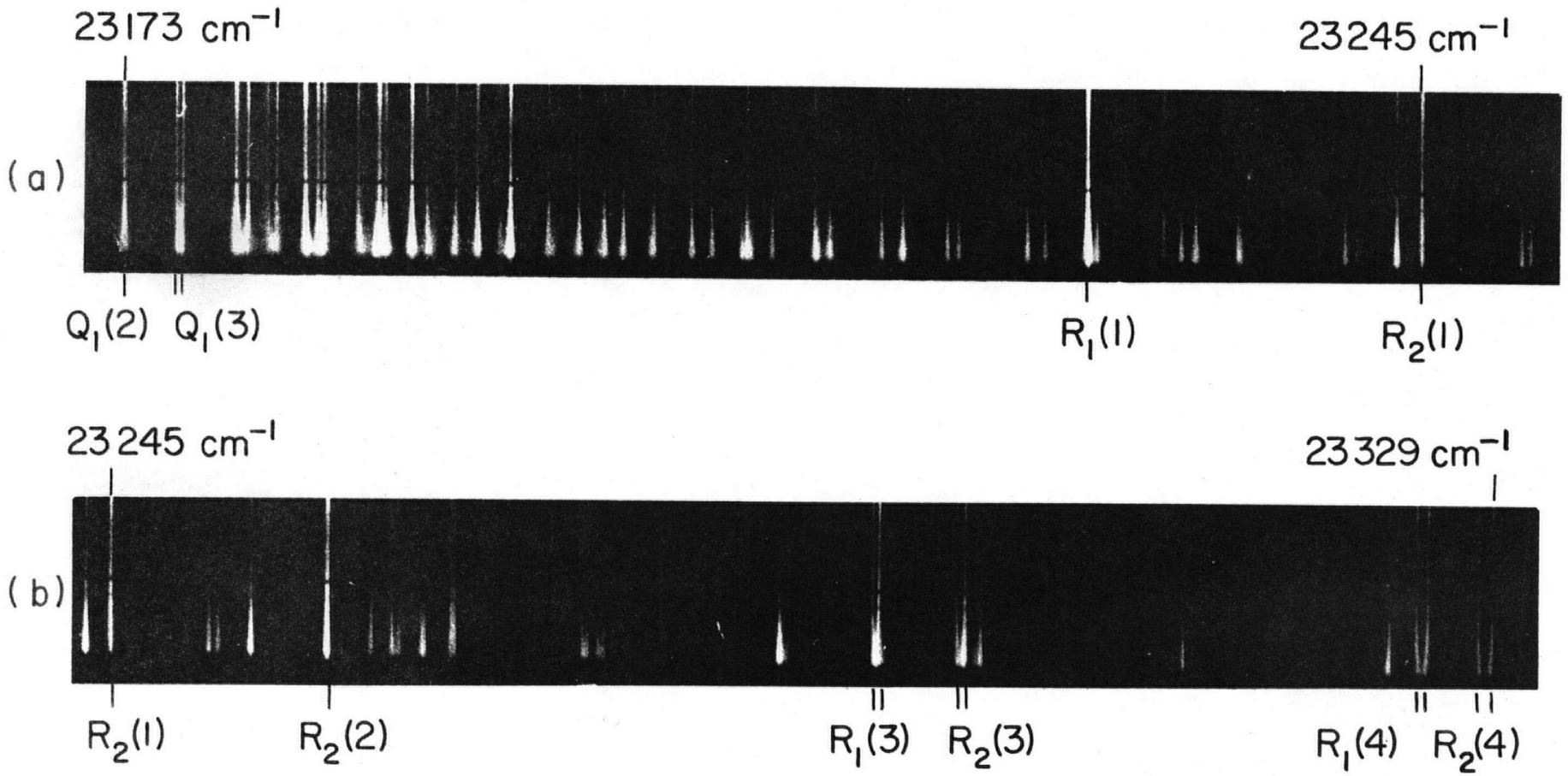

Figure 4.8. Stark effect on CH $^2\Delta \rightarrow {}^2\Pi$ band. Maximum electric field (near bottom of plate) is about 66 kV/cm. (Part (b) joins on the left of (a).)

on a portion of the CH $^2\Delta \rightarrow {}^2\Pi$, (0,0) band, $\lambda 4300\text{Å}$. The lines appearing in the enlargements belong to the Q_1, Q_2, R_1, and R_2 branches and extend from the $Q_1(2)$ lines to the $R_2(4)$ lines. (The (b) portion of the figure extends to the right (higher frequencies) from the right end of the (a) portion of the figure.) The region of maximum electric field is at the bottom of the lines on the print. The maximum field is about 66 kV/cm. The observed lines result from transitions from a lambda doublet rotational level in the $^2\Delta$ electronic state to one in the $^2\Pi$ electronic state. The lambda doubling in the $^2\Delta$ state is negligible[4] while that in the $^2\Pi$ state produces resolved doublets in the absence of an electric field. Compare for example the lines marked $Q_1(2)$ and $Q_1(3)$.

For the CH $^2\Delta \rightarrow {}^2\Pi$ band the lambda doublets in both the upper and lower state will be perturbed by the electric field and a large number of Stark components will result even for a transition between levels with low values of J. (Figure 2.5 in Chapter II shows the strong Stark transitions for the CH $Q_{1c}(3)$ and $Q_{1d}(3)$ lines.) As we see from the print in Figure 4.8 the Stark effect on the CH $^2\Delta \rightarrow {}^2\Pi$ band does cause lines to shift and broaden but because of the large number of closely spaced Stark components, no individual splittings could be resolved. We also see from this print that the $Q_{1c}(3)$ and $Q_{1d}(3)$ lines move together in the high field region as has been predicted. This is because the higher frequency Stark component of the low frequency line, $Q_{1c}(3)$, and the lower frequency Stark component of the high frequency line, $Q_{1d}(3)$, are the strong ones. Thus

these two lines cross in the region of high electric field. We will see below that the observation of the Stark effect on the CH $Q_{1c}(3)$ and $Q_{1d}(3)$ lines is sufficient to determine the relative sign of the dipole moments in the $^2\Delta$ and $^2\pi$ states and to determine the electric dipole moment of the CH molecule in its $^2\Delta$ excited electronic state.

Experimental conditions for spectrograms

To close the discussion of the spectrograms, Table I is included and lists the essential experimental conditions for the photographs appearing in Figures 4.2 through 4.8. The table provides the following information: The exposure number is that marked on the original photograph and on the data book entry. V is the voltage (in kilovolts) across the discharge tube. I is the current (in milliamperes) through the discharge tube. The total pressure in the discharge tube is p (in mm Hg) and the exposure time to the nearest tenth of an hour is t. The gas or gases used to produce the spectra and the cathode diameter and material forming it are also given. The electric fields were determined from Balmer H_γ Stark splittings for the OH plates and from CH or OH Stark splittings for the other exposures used as illustrations.

Measurements

Table II lists the measured values for the resolved first order Stark splittings observed in the OH, $^2\Sigma^+ \rightarrow {}^2\pi$ band and the corresponding Stark splittings for the atomic hydrogen Bal-

TABLE I

Experimental Conditions for Spectrograms used in Figures

Figure	Exposure Number*	V (kV)	I (ma)	p† (mm Hg)	t (hrs)	gas	Cathode‡	Electric Field× (kV/cm)
4.2	F - 10	3.0	3.4	0.9	1.5	H_2O	0.5mm Al	63
4.3	"	"	"	"	"	"	" "	"
4.4	"	"	"	"	"	"	" "	"
4.5	9/26/63 l	2.8	2.5	7.5	3.8	CH_3OH, He	0.5mm Al	52
4.6a	6/19/65 l	2.6	3.5	1.9	2.0	CH_3OH, He	1.0mm Al	34
4.6b	8/25/63 l	3.6	3.0	0.5	2.6	CH_3OH	1.0mm Al	47
4.6c	6/26/65 l	3.0	1.9	2.0	2.0	CH_3OH, He	0.5mm Al	68
4.7	1/20/65 l	3.5	3.0	1.9	3.8	CH_3OH, C_6H_{12}, He	1.0mm Al	36
4.8	6/28/65 u	3.6	1.9	2.8	1.3	CH_3OH, He	0.5mm Al	66

* u = upper, l = lower

† p is total pressure in discharge tube

‡ diameter of cathode in millimeters and metal used

× Electric field for CH $^2\Sigma \rightarrow {}^2\pi$ plates is determined from Stark splitting of CH $Q_2(1)$ line; field for CH $^2\Delta \rightarrow {}^2\pi$ plate is determined from Stark splitting of OH $P_{12}(1)$ line.

TABLE II

Observed Stark Splittings in OH $^2\Sigma^+ \rightarrow {}^2\pi$ Band
and in hydrogen Balmer H_γ line

Exposure No.	$R_2(1),(0,0)$ Δx(mm)	$R_2(1),(0,0)$ $\Delta\nu$(cm^{-1})	$P_{12}(1),(1,1)$ Δx(mm)	$P_{12}(1),(1,1)$ $\Delta\nu$(cm^{-1})	$P_1(1),(0,0)$ Δx(mm)	$P_1(1),(0,0)$ $\Delta\nu$(cm^{-1})	H_γ $\overline{\Delta x}$(mm)	H_γ E(kV/cm)
E-27 1	0.149±0.005	0.67_5±0.02	0.176±0.012	0.72_9±0.05*	0.135±0.007	0.61_5±0.03	0.84_5±0.02	34.9±0.8
E-22	0.230±0.003	1.04_3±0.01	0.242±0.003	1.00_3±0.01	0.201±0.009	0.91_6±0.04	1.19_1±0.06	49.2±2.4
6/23/63	0.232±0.006	1.05_2±0.02	———	———	0.213±0.007	0.97,±0.03	——— †	52.9±0.5
E-27 u	0.241±0.003	1.09_3±0.01	0.251±0.003	1.04_0±0.01	0.201±0.007	0.91_6±0.03	1.32_8±0.01	54.8±0.5
6/25/63	0.255±0.003	1.15_6±0.01	0.276±0.003	1.09_4±0.01	0.217±0.004	0.98_9±0.02	1.45_1±0.03 x	59.9±1.3
F-10	0.265±0.003	1.20_2±0.01	0.285±0.003	1.18_1±0.01	0.228±0.004	1.03_9±0.02	1.53±0.02 x	63.1±1.0

* This line was very weak. The error has been increased by a factor of 5 to take care of possible systematic errors in measurement.

† Field value from maximum Stark splitting of H_γ as measured on a prism spectrogram. Observed splitting was $112._2 \pm 1.0$ cm^{-1}.

x Uses only high frequency components. Corrections are made for second order Stark effects and changes in dispersion with frequency.

mer line H_γ. The splittings for the $R_2(1)$, (0,0) line and the $P_{12}(1)$, (1,1) line are between the $|M| = 1/2$ components. The splittings listed for the $P_1(1)$, (0,0) line are between the undisplaced line and the low frequency $|M| = 3/2$ component. These splittings are given in terms of the distance on the spectrographic plate measured in millimeters and also in terms of wave number units. The splittings are the average of eight measurements on each line. Four measurements were made by each of two observers. The $R_2(1)$, (0,0) line and the $P_{12}(1)$ line were chosen because they were free of overlapping. The $P_1(1)$, (0,0) was the only line arising from the lowest rotational level of $^2\Pi_{3/2}$ electronic state that had Stark components free of overlapping. The quantity $\overline{\Delta x}$ listed for the Balmer H_γ line and quoted in millimeters corresponds to a unit splitting of 0.0642 E cm^{-1}, where E is the magnitude of the electric field strength in kV/cm. This unit splitting is derived from measurements on five or more usually ten Stark components of H_γ. The ten H_γ Stark components were taken in corresponding pairs about the central line. In this way second order Stark effects cancelled out and the small linear change in wave number dispersion could be ignored. When only half of the Stark pattern was observed, corrections were made for second order Stark effects and for changing dispersion. The unit splitting was converted to wave numbers using a dispersion at H_γ of 2.65 cm^{-1}/mm.

Table III gives the observed and calculated positions of field induced-parity forbidden lines observed in the OH $^2\Sigma^+ \rightarrow {}^2\Pi$, (0,0) band. The measurements were made on a photo-

TABLE III

Observed and calculated positions of field-induced parity, forbidden-lines in the $^2\Sigma^+ \rightarrow {}^2\Pi$, (0,0), band of OH^+

	$P_1(K)$			$Q_1(K)$		
K	Calculated (cm^{-1})	Observed (cm^{-1})	Calc.-obs. (cm^{-1})	Calculated (cm^{-1})	Observed (cm^{-1})	Calc.-obs. (cm^{-1})
3	32 340.22	32 340.15	+0.07			
4	288.34	288.19	+0.15	32 424.41	32 424.61	-0.20
5	234.68	234.72	-0.04	404.75	404.77	-0.02
6	179.11	179.03	+0.08	382.71	382.77	-0.06
7	121.13	121.07	+0.06	358.29	358.11	+0.18
8	060.75	060.43	+0.32	331.05	331.39	-0.34
9				301.14	301.46	-0.32
10				268.00		
11				232.01	231.97	+0.04

* These forbidden lines are associated with the allowed lines: $P_1(K)$ and $Q_1(K)$. The calculated positions have not been corrected for shifts in energy due to the Stark effect.

† Measurements from exposure number F-10 which corresponds to an electric field of 63.1 kV/cm at maximum.

graphic plate for which the maximum electric field was (63.1 ± 1.0) kV/cm. These forbidden lines correspond to the P_1 and Q_1 allowed lines. The calculated positions were determined using the rotational levels given by Dieke and Crosswhite[1] for $^2\Pi_{3/2}$ state. The calculation ignores the small shift in energy due to the perturbation of the lambda doublets and makes the calculated position for the Q_1 line slightly higher than observed. (For example, the Stark shift would cause the deviation between calculated and observed values to be about 0.2 cm^{-1} for the $P_1(3)$ and less than 0.01 cm^{-1} for the $Q_1(1)$.)

Table IV lists the Stark splittings observed in the CH $^2\Sigma \rightarrow {}^2\Pi$, (0,0) band, λ 3900Å. These resolved first order Stark splittings were measured between the two $|M| = 1/2$ components of the $P_2(1)$ and $Q_2(1)$ lines. These Stark spectra were photographed in second order simultaneously with the Stark effect on the hydrogen Balmer line H_γ from which the electric field was determined. The CH Stark splittings are given in terms of the distance in millimeters measured on the spectroscopic plate and in terms of wave number units. The quantity $\overline{\Delta X}$ is the average value for a unit splitting of 0.0642 E cm^{-1}, where E is the magnitude of the electric field strength in kV/cm. On this plate the dispersion for H_γ was (5.54 ± 0.005) cm^{-1}/mm. Since the CH Stark splittings were small (and subsequently provided a value for the dipole moment to only ± 15%) the CH lines were measured four times each and the H_γ Stark components were measured twice pair-wise about the central line.

From the data listed in Table V a more accurate value of

TABLE IV

Observed Stark Splittings in CH $^2\Sigma \rightarrow {}^2\pi$ Band
and in hydrogen Balmer H_γ. (Observed in Second Order.)

	CH Stark Splittings				H_γ Splittings	
	$P_2(1)$		$Q_2(1)$			
Exposure No.	Δx (mm)	$\Delta \nu$ (cm^{-1})	Δx (mm)	$\Delta \nu$ (cm^{-1})	$\overline{\Delta x}$ (mm)	E(kV/cm)
2/16/65 u	$0.06_9 \pm 0.01$	0.51 ± 0.08	$0.05_9 \pm 0.01$	0.44 ± 0.08	$0.32_6 \pm 0.01$	$27._7 \pm 1.0$
2/13/65 u	$0.06_0 \pm 0.01$	0.44 ± 0.06	$0.06_2 \pm 0.01$	0.46 ± 0.06	0.354 ± 0.03	30 ± 3.0
1/ 3/65 m	———	———	$0.07_1 \pm 0.01$	0.54 ± 0.09	0.434 ± 0.01	37.4 ± 0.9
12/31/64 m	$0.10_0 \pm 0.01$	0.74 ± 0.07	$0.12_2 \pm 0.01$	0.90 ± 0.08	0.446 ± 0.01	38.3 ± 1.0
1/20/65 l	0.084 ± 0.01	0.62 ± 0.05	———	———	0.457 ± 0.005	39.3 ± 0.5
1/ 3/65 u	———	———	$0.09_3 \pm 0.01$	0.69 ± 0.08	$0.47_0 \pm 0.01$	$40._7 \pm 0.8$

u = upper

m = middle

l = lower

the CH electric dipole moment was derived. (The CH Stark splittings listed here were photographed in third order while those listed above were photographed in second order.) The Stark splittings listed in Table V for the CH $P_{12}(1)$, (0,0) line and the OH $R_2(1)$, (0,0) line were photographed simultaneously. Each Stark splitting was measured four times by two separate observers and an average of the eight measurements was taken. The OH Stark spectra were photographed in fourth order.

Table VI lists the experimental conditions for each experiment for which measured Stark splittings are given above. The table is in three parts and provides information for: (a) OH Stark splittings in the $^2\Sigma^+ \rightarrow {}^2\Pi$, (0,0) band photographed in fourth order, (b) CH Stark splittings in the $^2\Sigma^- \rightarrow {}^2\Pi$, (0,0) band photographed in second order, and (c) CH Stark splittings in the $^2\Sigma^- \rightarrow {}^2\Pi$, (0,0) band photographed simultaneously in third order with OH Stark splittings in the $^2\Sigma^+ \rightarrow {}^2\Pi$, (0,0) in fourth order. The CH $^2\Delta \rightarrow {}^2\Pi$, (0,0) band Stark spectra used to measure the electric dipole moment of the CH $^2\Delta$ electronic state were shown above as an illustration in Figure 4.7. The experimental conditions for that experiment are listed in Table I.

Analysis of Stark effect spectra

In Chapter II detailed expressions were given for the shift in frequency of a Stark effect component in electronic emission lines of a diatomic molecule. In this section the observed Stark splittings and shifts in energy which we have just

TABLE V

Simultaneously Observed Stark Splittings in CH and OH $^2\Sigma \rightarrow {}^2\Pi$ Bands

(CH and OH bands were observed in 3rd and 4th orders respectively.)

	CH, $P_{12}(1)$		OH, $R_2(1)$	
Exposure No.*	ΔX (mm)	$\Delta \nu$ (cm^{-1})	ΔX (mm)	$\Delta \nu$ (cm^{-1})
6/19/65 l	0.142 ± 0.010	$0.57_2 \pm 0.04$	0.167 ± 0.010 x	$0.70_2 \pm 0.04$ x
6/22/65 l	0.153 ± 0.007	$0.61_7 \pm 0.03$	0.167 ± 0.012	$0.71_4 \pm 0.05$
6/17/65 u	0.162 ± 0.005	$0.65_1 \pm 0.02$	0.174 ± 0.007	$0.74_5 \pm 0.03$
6/23/65 u	0.190 ± 0.005	$0.76_7 \pm 0.02$	0.220 ± 0.009	$0.94_0 \pm 0.04$

*u = upper, l = lower. x OH, $P_{12}(1)$

TABLE VI

Experimental Conditions for Plates Used to Determine OH and CH Electric Dipole Moments

(a) OH λ3064Å band (4th order), Hydrogen Balmer H_γ (3rd order)

Exposure* Number	V (kV)	I (ma)	p† (mm Hg)	t (hrs)	gas	cathode‡	Electric Field (kV/cm)
E-27 1	3.6	11.5	0.5	0.1	H_2O	2.0mm Al	34.9
E-22	3.7	4.5	4.5	0.7	"	1.0 W	49.2
6/23/63	6.3	3.2	0.8	1.8	"	1.0 Al	52.9
E-27 u	4.7	12.0	0.5	0.2	"	2.0 "	54.8
6/25/63	6.5	4.1	0.9	2.3	"	1.0 "	59.9
F-10	3.0	2.4	0.9	1.5	"	0.5 "	63.1

(b) CH λ3900Å band (2nd order), Hydrogen Balmer H_γ (2nd order)

2/16/65u	3.5	6.7	3.1	5.0	CH_3OH, He	1.0mm Al	27.7
2/13/65u	3.0	5.5	3.5	2.5	CH_3OH, He	" "	30
1/ 3/65m	4.0	6.0	0.55	3.0	CH_3OH	" "	37.4
12/31/64m	5.0	3.1	0.12	4.0	CH_3OH	" "	38.3
1/20/65l	3.5	3.0	1.9	3.8	(CH_3OH, C_6H_{12}, He)	" "	39.3
1/ 3/65u	4.0	5.0	0.40	1.5	CH_3OH	" "	40.7

(c) CH λ3900Å band (3rd order), OH λ3064Å band (4th order)

6/19/65l	2.6	3.1	1.9	2.1	CH_3OH, He	1.0mm Al	34.7
6/22/65l	3.0	3.5	1.5	1.0	" "	" "	36.5
6/17/65u	3.0	3.4	2.1	2.3	" "	" "	37.6
6/23/65u	4.1	3.5	1.5	1.7	" "	" "	47.1

* u = upper, m = middle, l = lower

† total pressure in discharge tube

‡ Cathode diameter in millimeters and material used

seen will be related to the appropriate mathematical expression. The main purpose of the section will be to provide an expression for the electric dipole moment of a molecule in a particular electronic state in terms of the observed Stark splitting or shift, the derived value of the electric field strength, and the quantum numbers of the rotational levels involved in the transition.

For the OH $^2\Sigma^+ \rightarrow {}^2\Pi$, $R_2(1)$, (0,0) and $P_{12}(1)$, (1,1) lines and for the CH $^2\Sigma^- \rightarrow {}^2\Pi$, (0,0) lines: $P_{12}(1)$, $Q_2(1)$ and $R_2(1)$, the Stark splittings correspond to the separation of two Stark components having the same value of $|M|$. We have seen in Chapter II that the energy of a lambda doublet Stark component relative to the center of the unperturbed doublet is given by:

$$\epsilon^1 = \pm \sqrt{(\lambda/2)^2 + (V_{12})^2}\,, \qquad (2.11)$$

where λ is the separation of the unperturbed doublet and V_{12} is the matrix element for the perturbation energy. The Stark splitting of interest corresponds to the difference of the positive and negative values of ϵ^1. That is the observed splitting can be written:

$$\Delta\nu = 2\sqrt{(\lambda/2)^2 + (V_{12})^2} \qquad (4.1)$$

All quantities are in wave number units. Solving for V_{12} gives:

$$2\,V_{12} = \sqrt{(\Delta\nu)^2 - \lambda^2}\,. \qquad (4.2)$$

For a $^2\Pi_{1/2}$, J = 1/2 level, M = 1/2 and Ω = 1/2 and $2\,V_{12} = 2\mu E\,(M\Omega/(J(J+1)))$ becomes:

$$2\,V_{12} = 2/3\mu E = \sqrt{(\Delta\nu)^2 - \lambda^2}\,, \qquad (4.3)$$

which will be referred to as the corrected splitting. Since the

$J = 1/2$ level of the $^2\Pi_{1/2}$ state always belongs to pure Hund's case (a) coupling there is no correction for intermediate coupling needed for expression (4.3).

It is convenient here to note the values for the lambda splitting needed to evaluate equation (4.3) for the $J = 1/2$ OH and CH lines listed above. For the OH $^2\Pi_{1/2}$, $J = 1/2$ level the lambda doubling was taken as $\lambda = 0.157$ cm^{-1} for OH in both the $v = 0$ and $v = 1$ vibrational state; the lambda for the CH $^2\Pi_{1/2}$, $J = 1/2$, $v = 0$ level was taken as $\lambda = 0.1135$ cm^{-1}. The value of the lambda doubling chosen for CH was determined by Douglas and Elliott[4] from high dispersion optical measurements of the CH $^2\Delta \rightarrow {}^2\Pi$ band. The value chosen for the OH lambda doubling was calculated using data obtained by Dousmanis, Sanders and Townes[5] from microwave absorption measurements. Since Dieke and Crosswhite[1] had obtained a value of 0.31 cm^{-1} for the OH lambda doubling from measurements of the ultraviolet spectrum an independent determination was made even though the lambda doubling computed from the microwave measurements was thought to be correct. The determination was made by measuring the Stark splitting for very small values of the electric field (at the top of the doublet). In the limit of zero electric field the Stark splitting is the lambda splitting. From observed Stark splittings a value of $\lambda = 0.15 \pm 0.03$ cm^{-1} was obtained and thus the microwave value of the lambda doubling was chosen.

For the electric fields used in this study second order Stark effects caused by neighboring rotational levels do not alter the analysis given above for splittings between Stark compo-

nents having the same value of $|M|$ since both components will be shifted by the same amount. For example, in the OH molecule second order effects in the $^2\Sigma$ state will cause a slight shift and a very slight separation of the M = 1/2 and M = 3/2 components of the rotational levels. For the $R_2(1)$ line, effects in the Σ state would broaden each doublet component by 0.007 cm^{-1} with essentially no shift at all. The $R_2(1)$ line arises from the K = 2, J = 3/2 rotational level. The other half of the spin doublet (K = 2, J = 5/2) does not result in transitions of appreciable intensity to the J = 1/2 ground state since mixing of the next lower ($^2\Sigma$, K = 1) level is always less than 1%. (These calculated values for second order effects do assume the dipole moment of the OH $^2\Sigma$ state is comparable to that found for the $^2\Pi$ ground state. But even if the dipole moment in the $^2\Sigma$ state were greater by a factor of two the mixing would only be doubled and the broadening would still be less than 0.03 cm^{-1}.) Similarly one finds that second order effects due to the rotational level adjacent to the J = 1/2, $^2\Pi_{1/2}$ level are negligible. The shift in frequency is the same for both Stark components of the lambda doublet and amount to only 0.013 cm^{-1} while the mixing of the J = 3/2 level of the $^2\Pi_{1/2}$ state is always less than 1.4%. Thus we can conclude that second order Stark effects do not effect the determination of the electric dipole moment from the doublet splitting of the OH $R_2(1)$ line.

Similarly second order Stark effects will not alter the separation of the CH doublet splittings which were used to determine the electric dipole moment from transitions to the

$J = 1/2$, $^2\Pi_{1/2}$ level. The CH $P_{12}(1)$ line which was used for the more accurate determination of the electric dipole moment will be discussed as an example. The observed transition arises from a single level ($^2\Sigma$, $K = 0$, $J = 1/2$) which will be shifted down by only 0.016 cm^{-1} and terminates at the lambda doublet ($^2\Pi_{1/2}$, $J = 1/2$) which is shifted down by only 0.014 cm^{-1}. The shifts which could be ignored individually are effectively cancelled. Mixing of adjacent rotational levels with the $J = 1/2$ levels will not broaden the observed Stark doublets. Thus we conclude that second order Stark effects do not effect the analysis of the CH Stark doublets observed here.

The electric dipole moment of the OH molecule in the $^2\Pi_{3/2}$ electronic state was determined from Stark splittings observed in the $P_1(1)$, (0,0) line. Since for this line the splitting was measured between the allowed line in zero electric field and the low frequency, $|M| = 3/2$, forbidden Stark component the analysis must include second order terms. The frequency of the $P_1(1)$ line for zero field can be written as $P_1(1) = F_1(0) - f_1'(1)$, where $F_1(0)$ is the term in the $^2\Sigma$ state and $f_1'(1)$ is the term for the lower lambda doublet level. In the presence of an electric field the upper and lower levels for the observed Stark component arises are:

upper state term: $F_1(0) - \varepsilon_\Sigma^2$.

lower state term: $f_1(1) + \lambda/2 + \sqrt{(\lambda/2)^2 + (V_{12})^2} - \varepsilon_\pi^2$.

The ε_Σ^2 and ε_π^2 are the second order shifts. The square root in the lower state term is the perturbed energy of the upper lambda

doublet level (termination of forbidden transition) measured from the center of the unperturbed lambda doublet; $f_1'(1) + \lambda/2$ then is the center of the unperturbed doublet. The forbidden transition will have a frequency found by the difference of the two perturbed terms, i.e.:

$$F_1(0) - \mathcal{E}_\Sigma^2 - (f_1'(1) + \lambda/2 + \sqrt{(\lambda/2)^2 + (V_{12})} - \mathcal{E}_\pi^2).$$

The observed splitting is the difference between this expression and that giving the frequency of the zero field $P_1(1)$ line. Thus we find the splitting is given by:

$$\Delta\nu(P_1(1)) = \lambda/2 + \sqrt{(\lambda/2)^2 + (V_{12})^2} + \mathcal{E}_\Sigma^2 - \mathcal{E}_\pi^2 . \qquad (4.4)$$

The value for the lambda doubling in the $J = 3/2$, $^2\Pi_{3/2}$ state is $\lambda = 0.0555$ cm^{-1} as determined by Ehrenstein[6] et. al. from microwave experiments. Since the lambda doubling is much less than the observed splitting the square root in equation (4.4) was expanded using the binomial expansion to give $V_{12} + (\lambda^2/8V_{12})$. The small correction to V_{12} was evaluated using the observed rather than the corrected splitting. The electric dipole moment was found from equation (4.4) by finding the corrected splitting: $\Delta\nu(P_1(1))$ - (corrections) = V_{12}. The matrix element, V_{12} was evaluated for intermediate coupling and the expression yielding the electric dipole moment was:

$$\text{Corrected splitting, } \Delta\nu' = V_{12} = \frac{(1.470)}{(1.500)} (3/5) \mu E \qquad (4.5)$$

The electric dipole moment of the CH molecule in the $^2\Delta$ electronic state was determined from the maximum shift in the high frequency component of the $Q_{1c}(3)$ line relative to the undisplaced line. The observed Stark effect on this line can only

be explained by assuming that the dipole moments in the upper and lower states have the same relative sign and that the maximum splitting in the upper state is slightly greater than in the lower state. (This situation was shown in the diagram in Figure 2.5) The shift in frequency of a Stark component relative to the zero field line is given by:

$$\Delta\nu(Q_{1c}(3)) = (V_{12})_{\Delta} - \sqrt{(\lambda/2)^2 + (V_{12})_{\pi}^2} + \lambda/2. \qquad (4.6)$$

The matrix elements for the upper and lower levels are labelled with subscripts and λ is the lambda doublet separation in the $^2\Pi$ state. (The lambda doubling in the $^2\Delta$ state is essentially zero[4] and therefore does not appear in equation (4.6).

Determination of electric dipole moments

The corrections given above were applied to the appropriate Stark splitting and the corrected splitting was plotted against the applied electric field. The slope was found using a least squares fit to a straight line through the origin. This slope is proportional to the electric dipole moment and provides the determined value. For example, Figure 4.9 shows a plot of corrected splitting vs. electric field for the OH $R_2(1)$ line in the $^2\Sigma^+ \rightarrow {}^2\Pi$, (0,0) band. In the figure the linear relationship between the corrected splitting and the applied electric field is observed as expected. The slope of the line is $(2/3\mu)$ in units of (1/kV) and is converted to a dipole moment in Debyes by multiplying by 3/2 and dividing by 0.01679 (kV/Debye).

Table VIII lists the observed and corrected Stark splittings and corresponding electric fields for the $R_2(1)$, (0,0);

$P_{12}(1)$, (1,1); and $P_1(1)$, (0,0) lines in the OH, $^2\Sigma^+ \rightarrow {}^2\Pi$ band. From these data the following values of the electric dipole moment of the OH molecule were obtained:

TABLE VII

OH Electric Dipole Moments Derived from Stark Splittings

Line	State	Dipole Moment (Debye)
$R_2(1)$, (0,0)	$^2\Pi_{1/2}$, v = 0	$1.73_2 \pm 0.02$
$P_1(1)$, (0,0)	$^2\Pi_{3/2}$, v = 0	$1.63_7 \pm 0.03$
$P_{12}(1)$,(1,1)	$^2\Pi_{1/2}$, v = 1	$1.69_2 \pm 0.04$

The errors quoted on the dipole moments in Table VII are standard deviations determined from the fit of the points to the line. On the basis of the observations one would expect that only the $P_1(1)$, (0,0) line would be effected by a systematic error. The observed Stark component of the OH $P_1(1)$, (0,0) line is close to a broad aluminum impurity line which might make the measured splitting too small and hence the derived dipole moment slightly too small. Also the value of the electric dipole moment derived from this $P_1(1)$ line depends slightly on the value assumed for the electric dipole moment of OH in the $^2\Sigma$ electronic state. If a value of the $^2\Sigma$ state dipole moment had been taken as half that of the $^2\Pi$ state, the value derived from the $P_1(1)$ line would be about 0.02 Debye higher. The $R_2(1)$, (0,0) and $P_{12}(1)$, (1,1) lines are completely free of blending so there is no apparent source of systematic error in the Stark splittings observed for these lines.

The electric dipole moment of the OH molecule has been de-

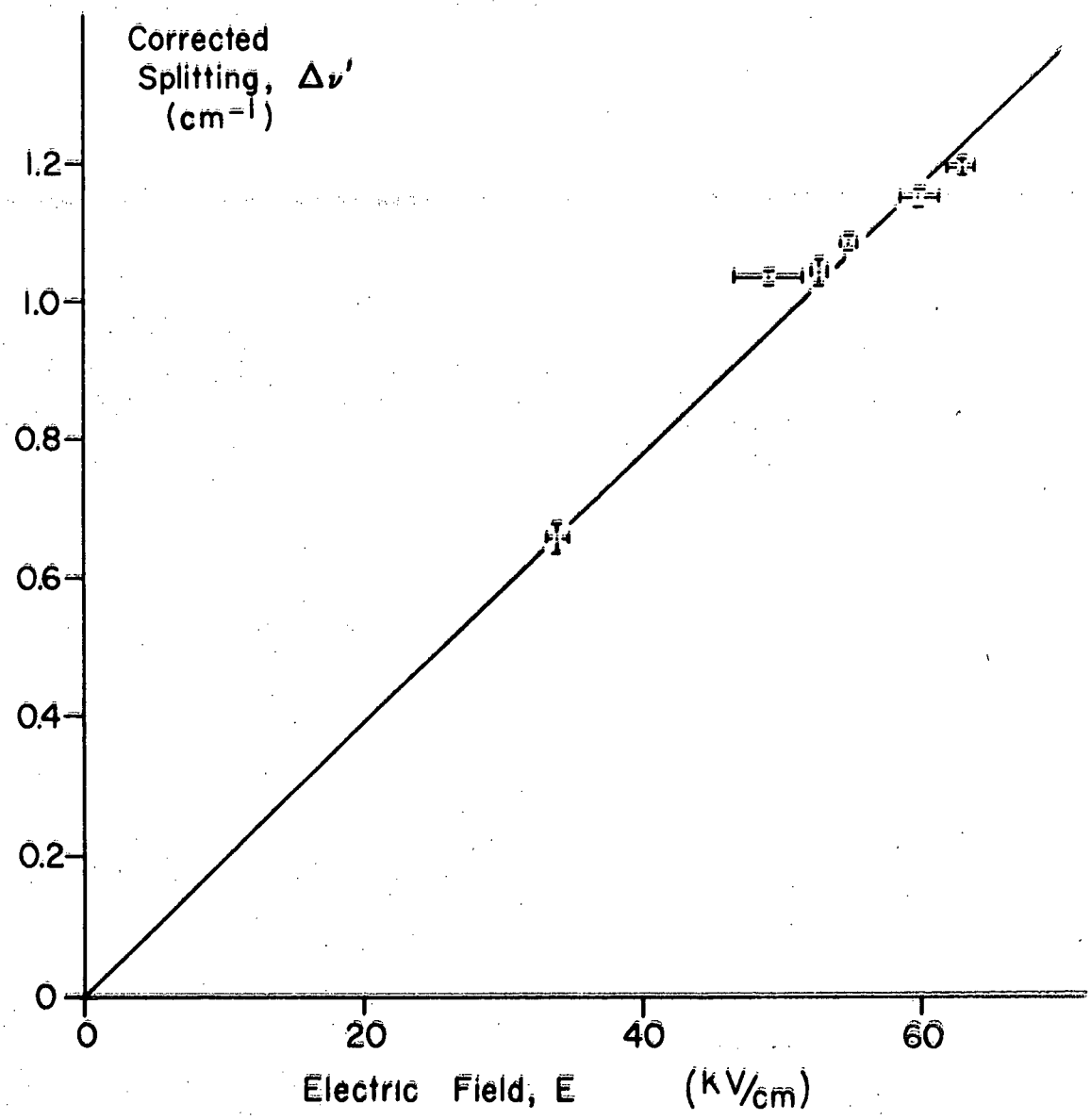

Figure 4.9. Corrected Stark splitting, $\Delta\nu'$, vs. electric field strength, E, for OH, $R_2(1)$, (0,0) line.

TABLE VIII

Corrected Stark Splittings in OH $^2\Sigma^+ \rightarrow {}^2\Pi$ Band*

	$R_2(1)$, (0,0)†		$P_{12}(1)$, (1,1)†		$P_1(1)$, (0,0)‡		
Exposure No.	$\Delta\nu$ (cm^{-1})	$\Delta\nu'$ (cm^{-1})	$\Delta\nu$ (cm^{-1})	$\Delta\nu'$ (cm^{-1})	$\Delta\nu$ (cm^{-1})	$\Delta\nu'$ (cm^{-1})	E(kV/cm)
E - 27 1	0.67_5	0.65_6	0.72_9	0.71_2	0.61_5	0.57_3	34.9
E - 22	1.04_3	1.03_1	1.00_3	0.99_1	0.91_6	0.86_3	49.2
6/23/63	1.05_2	1.04_0	———	———	0.97_1	0.91_4	52.9
E - 27 u	1.09_3	1.08_2	1.04_0	1.02_8	0.91_6	0.85_7	54.8
6/25/63	1.15_6	1.14_5	1.09_4	1.08_3	0.98_9	0.92_5	59.9
F - 10	1.20_2	1.19_1	1.18_1	1.17_1	1.03_9	0.97_8	63.1

*Experimental uncertainties are the same as given in Table II.

†Corrected for λ-type doubling in $^2\Pi_{1/2}$, J = 1/2 level using $\lambda = 0.157\ cm^{-1}$

‡Corrected for λ-type doubling in $^2\Pi_{3/2}$, J = 3/2 level using $\lambda = 0.0555\ cm^{-1}$ and for second order effects in $^2\Sigma$ and $^2\Pi_{3/2}$ states assuming dipole moment in each state is 1.7 Debye.

termined from microwave measurements. For purposes of discussion the most accurate value of (1.660 ± 0.010) Debye obtained by Powell and Lide[7] will be used. Their value is measured for the J = 7/2 level of the $^2\Pi_{3/2}$ state. (The earlier, less accurate microwave values obtained by Meyer and Myers[8] and by Ehrenstein[9] appear in Table XI found at the end of this chapter.) The electric dipole moment of the OH molecule has been computed for the electronic and vibrational ground state by Cade and Huo.[10] They obtained a value of 1.780 Debye. Cade and Huo have also computed the change in the electric dipole moment with internuclear distance. Using their computed values, the dipole moment is found to increase by 0.02 Debye for the 1.7% increase in internuclear distance in going from v = 0 to v = 1. The change in internuclear distance was found by using the formula given by Ramsey:[11]

$$(r - r_e)_v = r_e\left(\frac{\alpha_e}{2B_e} + \frac{3B_e}{\omega_e}\right)\left(v + \tfrac{1}{2}\right) \qquad (4.7)$$

where r is the internuclear distance and r_e is that at equilibrium, α_e is the vibrational correction at equilibrium and ω_e is the equilibrium vibrational constant.

We may now compare the values of the OH electric dipole moment given in Table VII with those found by Powell and Lide and by Cade and Huo. We can say immediately on the basis of Cade and Huo's calculation, that the value of the electric dipole moment determined from the Stark splitting of the $R_2(1)$, (0,0) line is too large by at least 0.03 Debye, and that the values obtained from the $P_1(1)$, (0,0) line and $P_{12}(1)$, (1,1) ap-

pear in the correct ratio. In turn the spectroscopic data suggests that the computed value of the OH dipole moment is about 0.1 Debye too large. The microwave value also suggests that the splitting measured in the $R_2(1)$, (0,0) line is too large. The standard deviation in the dipole moment given is a realistic measure of the fit of the Stark effect for $R_2(1)$,(0,0) line. Therefore, if the microwave value is correct, one must conclude the dipole moment found from the Stark splitting in the $R_2(1)$, (0,0) line is systematically high. However, the dipole moment found from the $R_2(1)$ line could be safely used to determine electric fields from measured values of Stark splittings in that line. The microwave value of the dipole moment and those values found from the Stark splittings of the $P_1(1)$,(0,0) line and the $P_{12}(1)$, (1,1) line are in good agreement. (The splittings in the $P_1(1)$ line are slightly low as anticipated above.)

The electric dipole moment of the CH molecule in the $^2\Pi$ electronic ground state was found by two independent experiments. The preliminary value of the dipole moment was found by measuring the Stark splittings of the $P_{12}(1)$, and $Q_2(1)$, (0,0) lines of the $^2\Sigma^- \rightarrow {}^2\Pi$ band observed in second order. The observed and corrected splittings and the corresponding electric fields are given in Table IX. The data were plotted and the slope of a line through the origin giving a least squares fit was found. (The slope was $2/3\mu$.) The value thus obtained for the electric dipole moment of the CH molecule in the $^2\Pi_{1/2}$ state was 1.45 Debye $\pm$ 15%.

A more accurate value of the electric dipole moment of the

TABLE IX

Corrected Low Dispersion Stark Splittings in CH $^2\Sigma^- \rightarrow {}^2\Pi$ Band*

	$P_{12}(1)$†		$Q_2(1)$		
Exposure No.✗	$\Delta\nu$(cm^{-1})	$\Delta\nu'$(cm^{-1})	$\Delta\nu$(cm^{-1})	$\Delta\nu'$(cm^{-1})	E(kV/cm)
2/16/65 u	0.51	0.49_9	0.44	0.42_6	27.7
2/13/65 u	0.44	0.42_8	0.46	0.44_6	30.0
1/ 3/65 m	——	——	0.54	0.52_6	37.4
12/31/64 m	0.74	0.73_2	0.90	0.89_3	38.3
1/20/65 l	0.62	0.61_4	——	——	39.3
1/ 3/65 u	——	——	0.69	0.68_4	40.7

*Experimental uncertainties are the same as given in Table IV

†Corrected for λ-type doubling using $\lambda = 0.1135$ cm^{-1}

✗u = upper, m = middle, l = lower

CH molecule was obtained from measurements of Stark splittings of the $P_{12}(1)$ line observed in third order. The electric field was determined from the OH, $R_2(1)$ line since no hydrogen Balmer line appeared on the photographic plates with sufficient intensity. The dipole moment was found by using the corrected splittings of simultaneously observed pairs of Stark lines (CH, $P_{12}(1)$ and OH, R (1)). The corrected splitting for each of these lines is $2/3\,\mu E$. A plot of the CH corrected splitting vs. OH corrected splitting appears in Figure 4.10. (The data are in Table X preceding the figure.) The slope of the line shown gives the ratio of the dipole moment of the CH molecule to the dipole moment of the OH molecule determined from the Stark effect on the $R_2(1)$ line. This treatment should effectively eliminate the small systematic error in the splitting of the $R_2(1)$ line. The slope of the line in Figure 4.10, found from a least square fit, is $(0.84_3 \pm 0.03_2)$. Using the value of the OH electric dipole moment (determined from the $R_2(1)$ line) of (1.73 ± 0.02) Debye the resulting value for the electric dipole moment of CH in the $^2\Pi_{1/2}$ electronic ground state is found to be (1.46 ± 0.06) Debye. The error quoted is a standard deviation resulting from the fit to the line and from the uncertainty in the derived value of the OH dipole moment. The CH splittings used here were slightly blended in two cases and this might result in a value of the CH electric dipole moment which was systematic high by 3%. The value of the CH electric dipole moment here can be compared with a value of 1.57 Debye computed by Cade and Huo.[10] Again the computed value is higher than that found

TABLE X

Corrected, Simultaneous Observed Stark Splittings in CH and OH $^2\Sigma \rightarrow {}^2\Pi$ Bands*

	CH, $P_{12}(1)^+$		OH, $R_2(1)^\ddagger$	
Exposure No.[x]	$\Delta\nu$ (cm^{-1})	$\Delta\nu'$ (cm^{-1})	$\Delta\nu$ (cm^{-1})	$\Delta\nu'$ (cm^{-1})
6/19/65 l	0.57_2	0.56_0	0.70_2	0.68_4
6/22/65 l	0.61_7	0.60_6	0.71_4	0.69_7
6/17/65 u	0.65_1	0.64_1	0.74_5	0.72_8
6/23/65 u	0.76_7	0.75_9	0.94_0	0.92_7

*Experimental uncertainties are the same as given in Table V.

†Corrected for λ-type doubling using $\lambda = 0.1135\ cm^{-1}$

‡Corrected for λ-type doubling using $\lambda = 0.157\ cm^{-1}$

[x] u = upper, l = lower

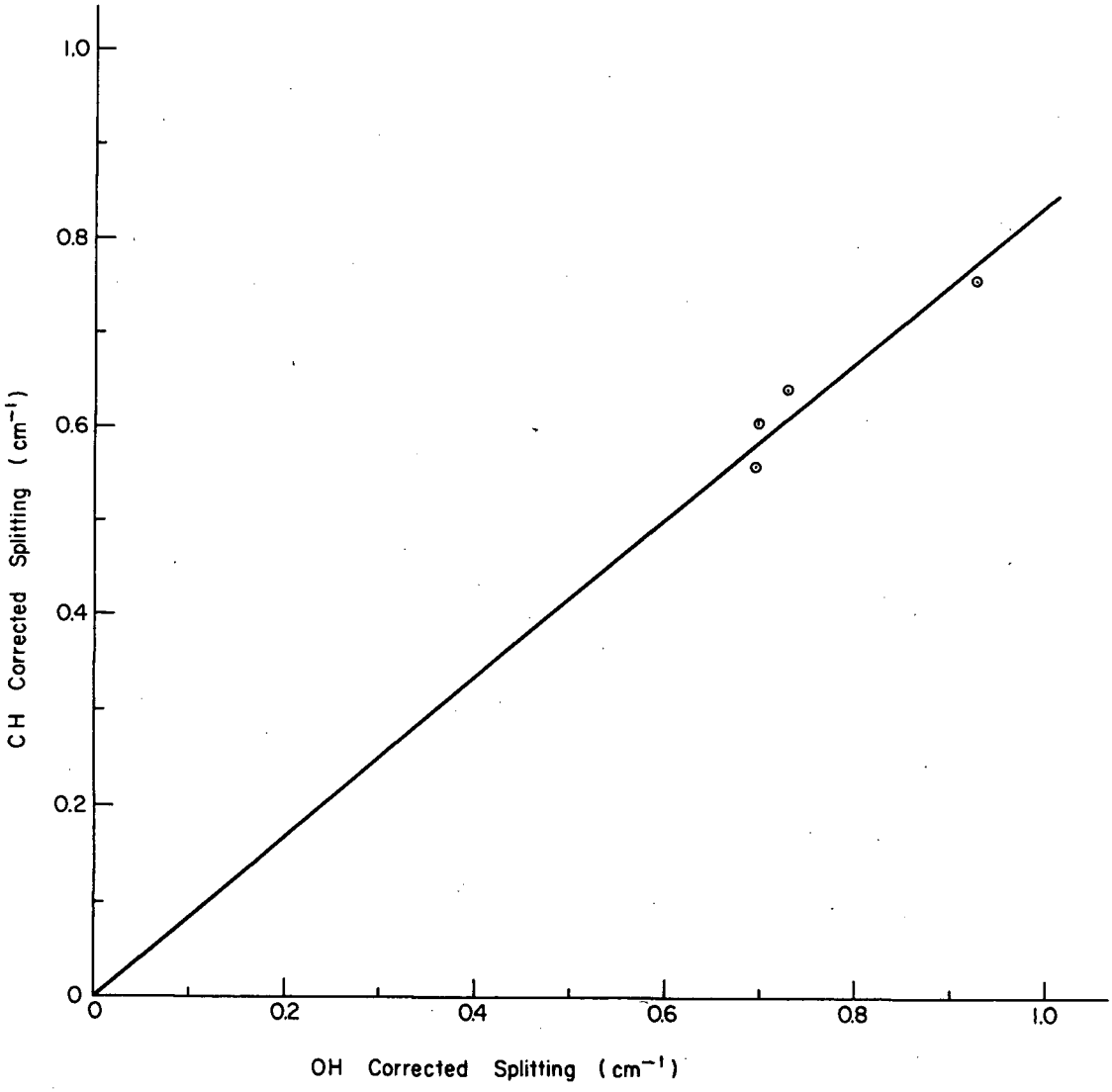

Figure 4.10. First-order Stark splitting of CH $P_{12}(1)$ line vs. first-order Stark splitting of OH $R_2(1)$ line. Splittings are corrected for lambda-type doubling.

by experiment. No other experimental values of the CH electric dipole moment exist for comparison with the value determined here.

The electric dipole moment of the CH molecule in the $^2\Delta$ electronic state was determined from the maximum observed Stark shift of the high frequency components of the $Q_{1c}(3)$ line in an electric field of 66 kV/cm. The maximum shift in frequency correspond to the separation of the $Q_{1c}(3)$ and $Q_{1d}(3)$ lines. This separation (which is also the required value of the lambda doubling) has been determined to be 0.373 cm^{-1} by Douglas and Elliott.[4] This value was used for calculation in preference to the earlier value of 0.38 cm^{-1} obtained by Gero.[2] The maximum shift in the Q_{1c} (3) line corresponds to the $|M| = 7/2 \rightarrow |M| = 5/2$ Stark component. The dipole moment of CH in the $^2\Delta$ state was found from equation (4.6) using J = 7/2, M = 7/2 in the upper state; J = 7/2, M = 5/2, and λ = 0.373 cm^{-1} in the lower state; an electric field of 66 kV/cm; and a maximum shift of (0.373 ± 0.06) cm^{-1}. The resulting value of the electric dipole moment of the CH molecule in the $^2\Delta$ electronic state is 1.13 Debye ± 15%. The uncertainty in this value is primarily due to the uncertainty in the value of the maximum shift in frequency of the $Q_{1c}(3)$ line.

Summary

In summary, the values for the electric dipole moments determined from observations of the Stark effect on the electronic emission spectra of the OH molecule ($^2\Sigma^+ \rightarrow {}^2\Pi$) and on

that of the CH molecule ($^2\Sigma^- \rightarrow {}^2\Pi$ and $^2\Delta \rightarrow {}^2\Pi$) are given below in Table XI. For comparison values of the electric dipole moment of OH as determined from microwave measurements are included. Computed values of the electric dipole moment of the OH and CH molecules are also given.

TABLE XI

Electric Dipole Moments for the OH and CH Molecules

Molecule	State	Dipole Moment (Debye)	Reference
OH	$^2\Pi_{3/2}$, J=9/2, v=0	1.65 ± 0.25	Meyer and Myers (1961)[8]
	$^2\Pi_{3/2}$, J=7/2, v=0	1.60 ± 0.12	Ehrenstein (1963)[9]
	$^2\Pi_{1/2}$, J=1/2, v=0	1.73_2 ± 0.02	This Work
	$^2\Pi_{3/2}$, J=3/2, v=0	1.63_7 ± 0.03	" "
	$^2\Pi_{1/2}$, J=1/2, v=1	1.69_2 ± 0.04	" "
	$^2\Pi_{3/2}$, J=7/2, v=0	1.660 ± 0.010	Powell and Lide (1965)[7]
	$^2\Pi$, v=0	1.780 (computed)	Cade and Huo (1965)[10]
CH	$^2\Pi_{1/2}$, J=1/2, v=0	1.46 ± 0.06	This work
	$^2\Pi$, v=0	1.57 (computed)	Cade and Huo (1965)[10]
	$^2\Delta$, J=7/2, v=0	1.13 ± 15%	This work

Footnotes for Chapter IV

1. G. H. Dieke and H. M. Crosswhite, Bumblebee Report No. 87 (John Hopkins University, 1948)

2. L. Gero, Z. Physik 118, 27 (1941).

3. E. U. Condon and G. H. Shortley, The Theory of Atomic Spectra (Cambridge University Press, Cambridge, England, 1935) p. 401.

4. A. E. Douglas and G. A. Elliott, Can. J. Phys. 43, 496, (1965).

5. G.C. Dousmanis, T. M. Sanders, and C. H. Townes, Phys. Rev. 100, 1732 (1955).

6. G. Ehrenstein, C. H. Townes, and M. J. Stevenson, Phys. Rev. Letters 3, 40 (1959)

7. F. X. Powell and David R. Lide, Jr., J. Chem. Phys. 42, 4201 (1965).

8. R. T. Meyer and R. J. Myres, J. Chem. Phys. 34, 1074 (1961).

9. G. Ehrenstein, Phys. Rev. 130, 669 (1963).

10. Private communication: Paul E. Cade and Winifred Huo, Laboratory of Molecular Structure and Spectra, Physics Department, University of Chicago, Chicago, Illinois.

11. N. F. Ramsey, Molecular Beams (Clarendon Press, Oxford, 1956), p. 231.

CHAPTER V

CONCLUSION AND SUGGESTIONS FOR FURTHER STUDY

This work has reported the first successful observation of linear Stark splittings produced in the electronic spectra of a diatomic molecule. The observations have also shown broadenings and field induced-parity forbidden lines resulting from the Stark effect. All these features are in agreement with the theoretical predictions for the Stark spectra of a diatomic molecule having a permanent electric dipole moment, when the observed electronic transitions involve at least one degenerate electronic state. Derived values are summarized at the end of the previous chapter. The electric dipole moment of the OH molecule in the $^2\Pi$ electronic state and of the CH molecule in the $^2\Pi$ and $^2\Delta$ electronic states are given there.

This work has shown that the techniques used here provide a means of determining the electric dipole moment for short lived and chemically reactive species. Furthermore, with these techniques the electric dipole moment of a molecule in excited electronic states have been determined.

Suggestions for further work

The most interesting topic for further study would be the fading of the forbidden Stark components of several low J lines observed in the CH, $^2\Sigma \rightarrow {}^2\Pi$, $\lambda 3900\text{Å}$ band for an electric field exceeding 120 kV/cm. Such a study would probably involve improving the stability of the cathode in the discharge tube. Per-

haps an alternative technique for producing large electric fields could be developed. However, adapting the present spectrograph for photoelectric detection may overcome the present low intensities encountered at very high electric fields. This would allow studies at high electric fields with the present discharge tube. Further study of the slight difference between the dipole moments deduced from different transitions going to the same electronic and vibrational state is advised for the OH, $^2\Sigma^+ \rightarrow {}^2\Pi$, $R_2(1)$ and $P_1(1)$ lines and for the CH, $^2\Sigma^- \rightarrow {}^2\Pi$, $P_2(1)$, $Q_2(1)$ and $R_2(1)$ lines. In doing this it would be important to give particular attention to eliminating sources of impurity lines.